Climate Data Record (CDR) Program

Climate Algorithm Theoretical Basis Document (C-ATBD)

AMSU Brightness Temperature – NOAA

AMSU Brightness Temperature – NOAA Gridded

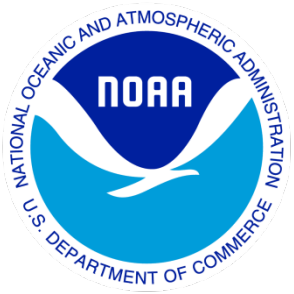

CDR Program Document Number: CDRP-ATBD-0345
Configuration Item Number: 01B-18 and 01B-18a
Revision 2 / May 31, 2016

REVISION HISTORY

Rev.	Author	DSR No.	Description	Date
1	Cheng-Zhi Zou, NOAA/NESDIS Wenhui Wang, I.M. Systems Group	DSR-402	Initial Submission to CDR Program	02/27/2012
2	Cheng-Zhi Zou, NOAA/NESDIS Xianjun Hao, George Mason University	DSR-1045	Added algorithm description on the AMSU-A daily gridded FCDR	05/31/2016

TABLE of CONTENTS

LIST of FIGURES

LIST of TABLES

1. Introduction

1.1 Purpose

The purpose of this document is to describe the algorithm submitted to the National Centers for Environmental Information (NCEI) by Cheng-Zhi Zou at NOAA/NESDIS/Center for Satellite Applications and Research that will be used to create the radiance Fundamental Climate Data Record (FCDR), using the Microwave Sounding Unit (MSU) and Advanced Microwave Sounding Unit-A (AMSU-A). The actual algorithm is defined by the computer program (code) that accompanies this document, and thus the intent here is to provide a guide to understanding that algorithm, from both a scientific perspective and in order to assist a software engineer performing an evaluation of the code.

1.2 Definitions

Radiance: Satellite observation of the radiation emitted to space from the earth and the atmosphere; it is converted from raw counts data of satellite observations using instrument calibration equation.

Brightness Temperature: Satellite observation at the top of the atmosphere at each scan position; it is converted from Radiance using the Planck Function with instrument channel frequency as the input.

Correction of Sensor Incidence Angle Effect (or Limb Correction): It adjusts brightness temperatures measured at off-nadir viewing angles to those at nadir views. Statistical techniques and model simulations were both employed for limb-corrections in the AMSU-A observations. Details are shown in relevant sections.

Level-1C data: Orbital data containing calibrated swath radiances at scan positions as well as other satellite geo-location and calibration information taken from satellite Level-1b files. The Level-1c data as described in this document is calibrated by the Integrated Microwave Inter-Calibration Approach (IMICA).

The following is a summary of the symbols used to define the IMICA calibration algorithm.

MSU/AMSU level-1c calibration equation and parameters:

$$R = R_L - \delta R + \mu Z \tag{1-1}$$

where

R = Earth scene radiance

$R_L = R_c + S(C_e - C_c)$ *= Earth scene radiance from the linear calibration*

$Z = S^2(C_e - C_c)(C_e - C_w)$ *= Non- linear response*

$S = \frac{R_w - R_c}{C_w - C_c}$ *=Slope determined by the space cold and onboard blackbody warm calibration targets*

R_w *=Radiance of the onboard blackbody warm target*

R_c *= Radiance of the cosmic space cold target*

C_e *= Raw counts data from the Earth view*

C_w *= Raw counts data from the warm target view*

C_c *= Raw counts data from the cold target (cosmic space) view*

δR*= Calibration offset (determined by post-launch calibration)*

μ*= Non-linear calibration coefficient (determined by post-launch calibration)*

Supplemental simultaneous nadir overpass (SNO) regression algorithm for obtaining calibration coefficients:

$$\Delta R = \Delta R_L - \Delta \delta R + \mu_k Z_k - \mu_j Z_j \quad (1\text{-}2)$$

where

$\Delta R = R_k - R_j$

$\Delta R_L = R_{L,k} - R_{L,j}$

$\Delta \delta R = \delta R_k - \delta R_j$

k and j = satellite index referring to satellites k and j, respectively

Z_k *and* Z_j *= Non-linear responses for satellites k and j, respectively*

μ_k, *and* μ_j *= Non-linear coefficients for satellites k and j, respectively*

Equation 1-1 provides the level-1c radiance FCDR with given variables from observations except for δR and μ. The regression algorithm (Equation 1-2) obtains values of three calibration coefficients, $\Delta \delta R$, μ_k, and μ_j using SNOs with a strong constraint that the instrument temperature variability in the calibrated radiances is minimal. A sequential procedure is then applied to obtain calibration coefficients for all recalibrated satellite channels. Equation 1-1 is the main algorithm for the data processing described in this document. Equation 1-2 is an offline supplement to Equation 1-1 which helps the readers to understand how the calibration coefficients are obtained. Equation 1-2 is not part of the

processing code described in this document. Details on how to solve for the calibration coefficients are described in the Algorithm Section.

Level-3 data or Daily Gridded FCDR: Gridded brightness temperature dataset generated from Level-1C data for individual satellite channels. In this case, the orbital swath data at scan positions are binned into grid cells with grid resolution of 1.0° latitude by 1.0° longitude at daily interval. The binned data at grid cells are then averaged to derive the daily gridded brightness temperature FCDR.

1.3 Referencing this Document

This document should be referenced as follows:

AMSU-A Brightness Temperature FCDR - Climate Algorithm Theoretical Basis Document, NOAA Climate Data Record Program CDRP-ATBD-0345, Rev. 2.0 (2016). Available at http://www.ncdc.noaa.gov/cdr/operationalcdrs.html

1.4 Document Maintenance

The algorithm has been used to inter-calibrate all atmospheric temperature sounding channels of MSU/AMSU-A instruments. The main products of the algorithm are calibration coefficients and their resulting radiance FCDR datasets. Two changes may occur to the algorithm and its resulting datasets: major changes to the theoretical basis of the calibration algorithm and update of the resulting calibration coefficients and their associated FCDR dataset. The first change is not expected to occur frequently since the calibration theory and equations are fairly mature. However, if a change does occur, the document will be rewritten to include the new theory and results.

The second change is expected to occur more frequently. This is because satellite data inter-calibrated before need to be recalibrated in a routine (e.g. yearly) basis when new observations such as those from the Advanced Technology Microwave Sounder (ATMS) onboard Suomi National Polar-orbiting Partnership (Suomi NPP) and to be flown on Joint Polar Satellite System (JPSS) are available. Recalibration will provide updated calibration coefficients and radiance FCDR datasets that include new satellite observations. These updates will be documented as supplements to this document. After a substantial set of satellite channels are recalibrated, version update for the document will be provided to include results of the newly inter-calibrated satellite channels.

2. Observing Systems Overview

This section provides an overview of characteristics of the MSU/AMSU observing systems and its calibration strategy. It also describes radiance FCDR requirements and characteristics generated by the MSU/AMSU-A inter-calibration algorithm.

2.1 Products Generated

The Integrated Microwave Inter-Calibration Approach (IMICA, also known as SNO inter-calibration algorithm) generates swath level-1c radiance data at each scan position on the MSU/AMSU-A scan-lines. The MSU and AMSU-A have respectively 11 and 30 field of views (FOVs) on each scan-line. Table 2-1 and Table 2-2 respectively list the requirements and characteristics for the radiance MSU and AMSU-A FCDR datasets derived from the IMICA inter-calibration.

Table 2-1 Requirements on the radiance FCDR from the MSU Observations. Due to a linear relationship between the radiances and brightness temperatures in the microwave soundings, the requirements are provided with respect to the brightness temperature measurements.

Radiance FCDRs from MSU	Requirement
Product Geographic Coverage/Conditions	Global coverage except for heavy precipitation
Product Vertical Resolution (km)	Radiance products represent atmospheric layer temperatures; Vertical resolution represented by channel weighting functions is 3 to 5 km
Product Horizontal Resolution (km)	110 km at nadir to 320 km at limb
Product Measurement Range (K)	180 K– 320 K
Product Absolute Calibration Accuracy (K) (relative to assumed SI-Traceable Standards)	1K
Product Relative Calibration Accuracy (K) (relative to the same MSU measurement but onboard different satellites)	Operational Calibration: 1K IMICA Inter-Calibration: 0.1-0.2K
Product Refresh Rate/Coverage Time	Global coverage: 1 day
Product length	28 years (Nov. 1978-Sep. 2006)
Step time per measurement	1.84 seconds
Product Calibration Precision (K)	0.03-0.05 K in global mean for IMICA calibration; 0.15-0.20K in global mean for operational calibration

Table 2-2 Same as Table 2-1 except for AMSU-A instrument.

Radiance FCDRs from AMSU	Requirement
Product Geographic Coverage/Conditions	Global coverage except heavy precipitation
Product Vertical Resolution (km)	Radiance products represent atmospheric layer temperatures; Vertical resolution represented by channel weighting functions is 1 to 3 km
Product Horizontal Resolution (km)	45 km at nadir
Product Measurement Range (K)	180 – 320K
Product Absolute Calibration Accuracy (K) (relative to assumed SI-Traceable Standard)	0.5-1K
Product Relative Calibration Accuracy (K) (relative to the same AMSU measurement but onboard different satellites)	Operational Calibration: 0.5-1K IMICA Inter-Calibration: 0.1-0.2K
Product Refresh Rate/Coverage Time	Global coverage: 1 day
Product length	18 years (Oct. 1998-present)
Step time per measurement	0.2 seconds
Product Calibration Precision (K)	0.03-0.05 K in global mean for IMICA calibration

In addition to the level-1c swath data, AMSU-A daily gridded brightness temperature FCDR products were generated, including 11 channels (4-14) of AMSU-A from 6 polar orbiting satellites onboard NOAA-15 through NOAA-18, MetOp-A, and EOS Aqua, for both ascending and descending orbits, respectively. Requirements on the gridded daily AMSU-A brightness temperature products are shown in table 2-3. Since the gridded FCDR products are based on the AMSU-A level-1c radiance FCDR products, most technical specifications follow the AMSU-A radiance FCDR products except for the horizontal resolution and refresh rate.

Table 2-3 Requirements on gridded daily AMSU-A brightness temperature FCDR.

Gridded Daily AMSU-A brightness temperature FCDR	Requirements
Product geographic coverage/conditions	Global coverage except heavy precipitation
Product horizontal resolution	1 degree
Gridding strategies	1. Using FOVs at near-nadir only 2. Using FOVs with minimum viewing zenith angle 3. Average of multiple FOVs in a scan-

	line
Product vertical resolution	Vertical resolution represented by channel weighting functions is 1 to 3 km
Product measurement range	180-320K
Product absolute calibration accuracy (relative to assumed SI-Traceable Standard)	0.5-1K
Product relative calibration accuracy (relative to the same AMSU-A measurement but onboard different satellites)	Operational calibration: 0.5-1K IMICA inter-calibration: 0.1-0.2K
Product refresh rate/coverage time	Global coverage: around 1 month for near-nadir FOVs only, around 1 week for FOV with minimum viewing zenith angle and average brightness temperature of FOVs from multiple scan positions. Precise refresh rate depends on individual satellites.
Product length	18 years (October 1998 – present)

The three gridding strategies in Table 2-3 result in three different products as defined below:

1. **Brightness temperatures of near-nadir FOVs only:** Only near-nadir pixels (scan positions 15 and 16) from IMICA FCDR products are used to compose daily products. In case more than one near-nadir pixels are accumulated in one grid cell, their average is used to represent the daily brightness temperatures for the grid cell.

2. **Brightness temperature of FOV with minimum viewing zenith angle:** For each grid cell, pixels from multiple scan positions (8-23) are collected; but the brightness temperatures from the IMICA FCDR products for the FOV with minimum viewing angle is selected to represent the grid cell. Corresponding time is also included in the product.

3. **Average brightness temperatures of FOVs from multiple scan positions:** For each grid cell, pixels from multiple scan positions (8-23) are collected, and the average brightness temperature of these pixels from limb-corrected IMICA FCDR product is used to represent the cell. Corresponding standard deviation is also included in the product.

The gridded datasets have spatial resolution of 1°x1°, and cover the time period from Oct. 1998 to present for ascending and descending orbits, respectively. Other necessary metadata are also included in the products. Figures 2-1 to 2-6 illustrate examples of the daily gridded AMSU-A FCDR products. Primary contents of the products are listed in tables 2-4 to 2-6.

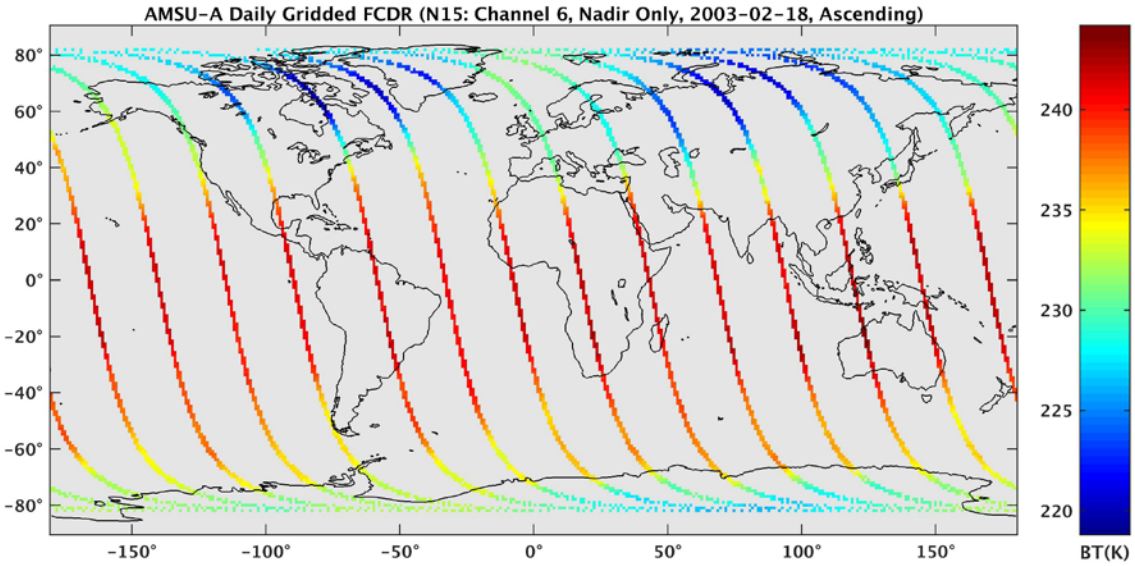

Figure 2-1 Daily gridded near-nadir-only FCDR (ascending node) for NOAA-15 AMSU-A channel 6 on 02/18/2003.

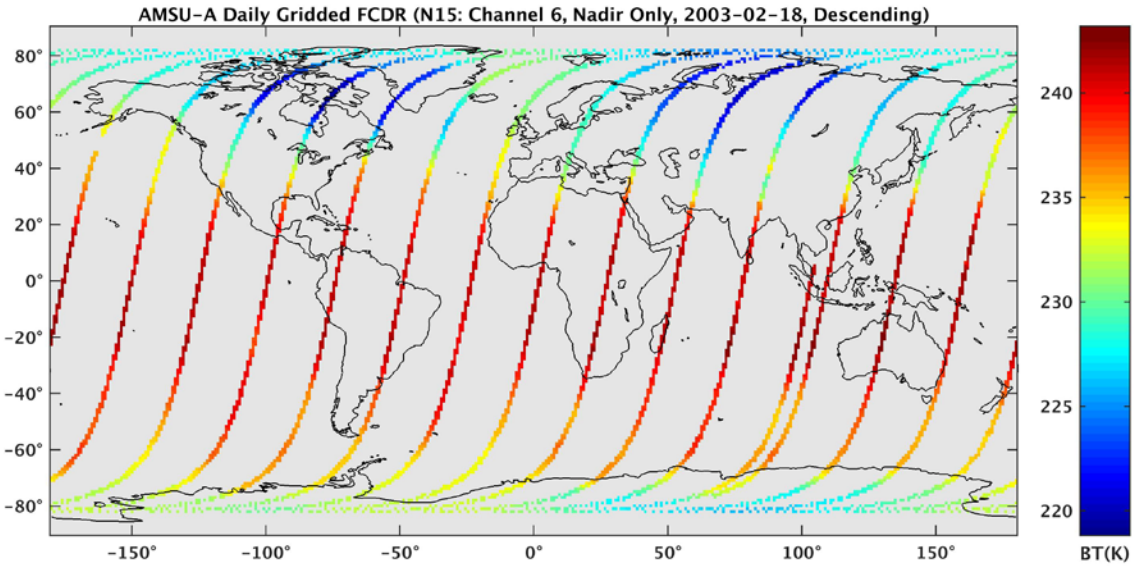

Figure 2-2 Daily gridded near-nadir-only FCDR (descending) for NOAA 15 AMSU-A channel 6 on 02/18/2003.

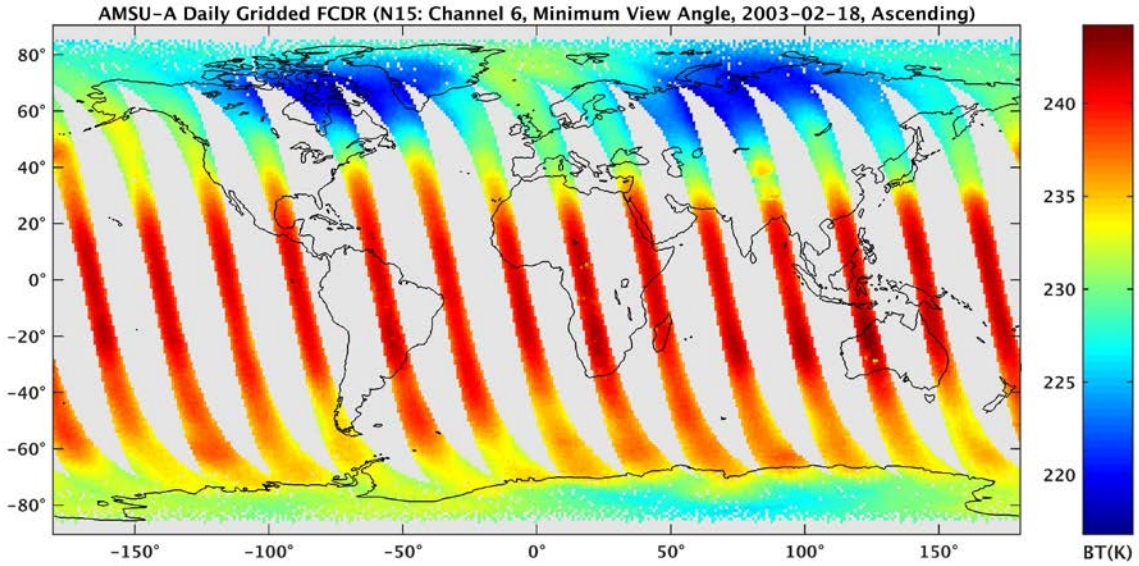

Figure 2-3 Daily gridded minimum-view-angle (ascending) for NOAA 15 AMSU-A channel 6 FCDR on 02/18/2003.

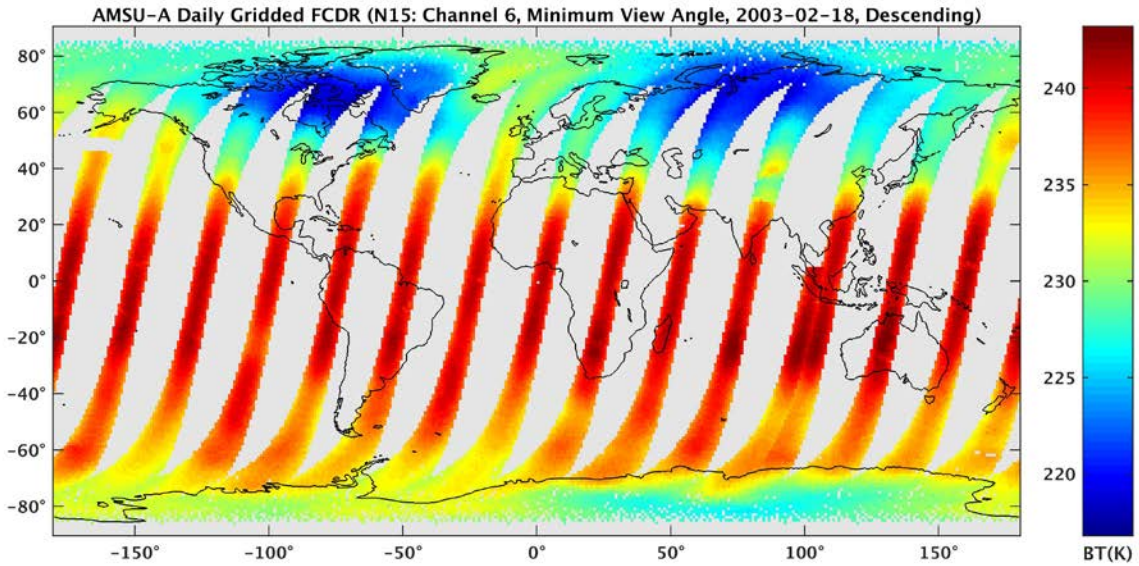

Figure 2-4 Daily gridded minimum-view-angle (descending) for NOAA 15 AMSU-A channel 6 FCDR on 02/18/2003.

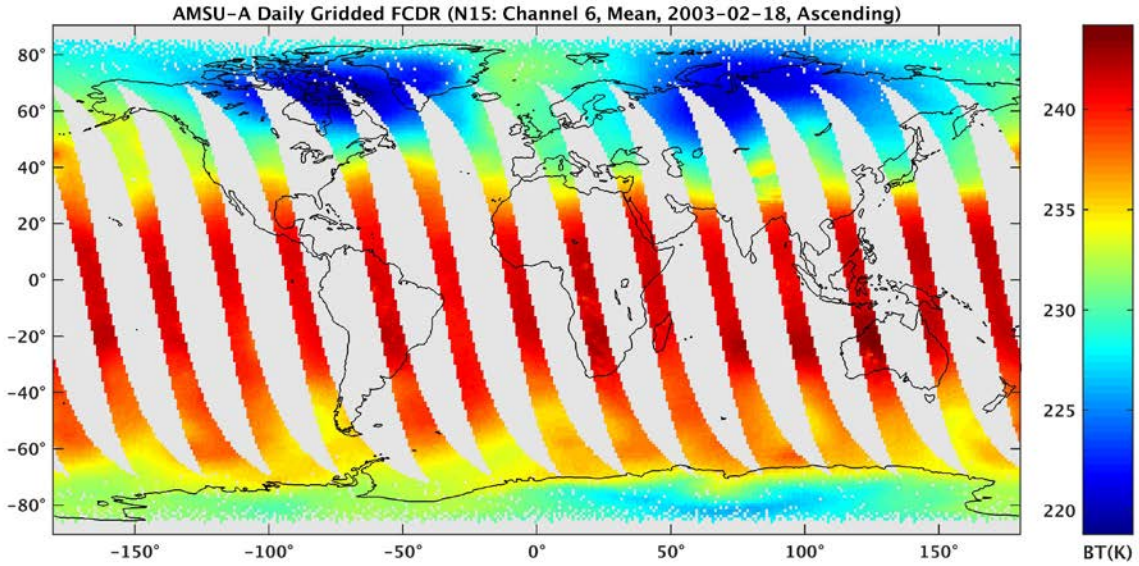

Figure 2-5 Daily gridded mean (ascending) FCDR for NOAA 15 AMSU-A channel 6 on 02/18/2003.

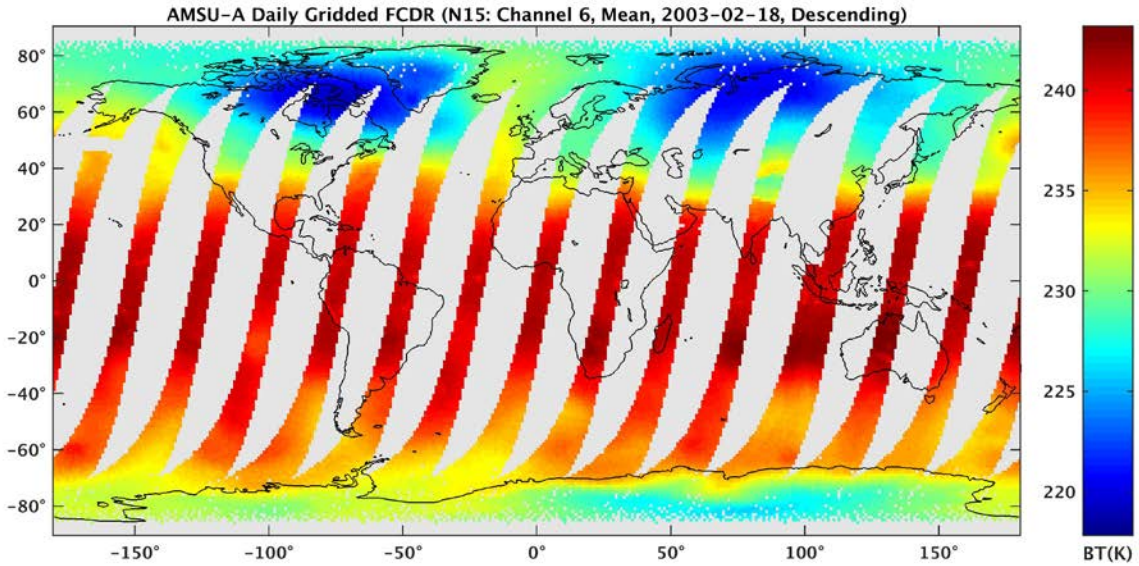

Figure 2-6 Daily gridded mean (descending) FCDR for NOAA 15 AMSU-A channel 6 on 02/18/2003.

Table 2-4 List of content in the daily near-nadir only AMSU-A brightness temperature products for ascending and descending orbits.

Products Contents	Description
BT_chX_IMICA _ascending_nadir; (chX goes from ch4 through ch14)	Gridded daily brightness temperature of AMSU-A channel X from near-nadir pixels only of the ascending orbit; where channel X goes from channels 4 through 14
BT_chX_IMICA _descending_nadir; (chX goes from ch4 through ch14)	Gridded daily brightness temperature of AMSU-A channel X from near-nadir pixels only of the descending orbit; where channel X goes from channel 4 through channel 14

Table 2-5 List of content in the daily minimum-view-zenith-angle AMSU-A brightness temperature products for ascending and descending orbits.

Products Contents	Description
BT_chX_IMICA _ascending_minvza (chX goes from ch4 through ch14)	Gridded daily brightness temperature of AMSU-A channel X from pixels with minimum view zenith angles of ascending orbit; where channel X goes from channel 4 through channel 14
time_IMICA_minvza_since_1978_ascending	Time of selected pixel since 1978 (in seconds)
view_zenith_angle_IMICA_ascending	View zenith angle of the selected pixel
BT_chX_IMICA _descending_minvza (chX goes from ch4 through ch14)	Gridded daily brightness temperature of AMSU-A channel X from pixels with minimum view zenith angles of descending orbit; where channel X goes from channel 4 through channel 14
time_IMICA_minvza_since_1978_descending	Time of selected pixel since 1978 (in seconds)
view_zenith_angle_IMICA_descending	View zenith angle of the selected pixel

Table 2-6 List of content in the gridded daily mean AMSU-A brightness temperature products for ascending and descending orbits.

Products Contents	Description
BT_chX_IMICA_ascending_mean (chX goes from ch4 through ch14)	Gridded daily average brightness temperature of AMSU-A channel X of pixels from multiple scan positions (8-23) in a scan-line of ascending orbit; where channel X goes from channel 4 through channel 14
BT_ch4_IMICA_ascending_std (chX goes from ch4 through ch14)	Standard deviation of AMSU-A channel X brightness temperature of pixels from multiple scan positions (8-23) in a scan-line of ascending orbit; where channel X goes from

	channel 4 through channel 14
BT_chX_IMICA_descending_mean (chX goes from ch4 through ch14)	Gridded daily average brightness temperature of AMSU-A channel X of pixels from multiple scan positions (8-23) in a scan-line of descending orbit; where channel X goes from channel 4 through channel 14
BT_ch4_IMICA_descending_std (chX goes from ch4 through ch14)	Standard deviation of AMSU-A channel X brightness temperature of pixels from multiple scan positions (8-23) in a scan-line of descending orbit; where channel X goes from channel 4 through channel 14

2.2 Instrument Characteristics

MSU and AMSU-A are both cross-track, line-scanned instruments designed to measure Earth scene radiances. The detailed system parameters and measurement principles for MSU and AMSU-A can be found in Kidwell (e.g., 1998) and Robel et al. (2009). Here only the instrument characteristics related to the IMICA inter-calibration and FCDR development are briefly described.

2.2.1 MSU

MSU is a microwave Dicke radiometer with four-channels to make passive measurements in the 5.5 millimeter oxygen region. The four channels respond to the following respective spectral frequencies: 50.3, 53.74, 54.96, and 57.95 GHz with a channel bandwidth of 200 MHz in each case, and a typical NEΔT of 0.3K. The MSU sensors consist of two four-inch diameter antennas named as MSU-1 and MSU-2, respectively. Each of the two antennas has an IFOV of 7.5 degrees. The MSU-1 is used by channels 1 and 2 while MSU-2 by channels 3 and 4. The antennas are step-scanned through eleven individual 1.84-second Earth viewing steps and require a total of 25.6 seconds to complete.

The MSU instrument uses an on-board calibration method that includes two calibration targets as its end point references: the cosmic space cold target and an onboard blackbody warm target. The cold space has a temperature of 2.73 K, and the warm target temperature is measured by the platinum resistance thermometers (PRT) embedded in the blackbody target. There are 2 PRTs embedded on the blackbody target. The antennas view the cold target and the warm target once during each scan cycle. The signals from the Earth views and target views in the form of electric voltage are converted to digital counts through an analog-to-digital converter, which are output as the raw observations. The MSU level-1c calibration converts the raw counts data of the 11 Earth views to radiances using the one cold and one warm target views as references in each scan-line.

The MSU instrument parameters can be found in Kidwell (1998) and are also summarized in Table 2-7.

Table 2-7 MSU instrument parameters.

Cross-track scan angle (degrees from nadir)	± 47.35
Scan time (seconds)	25.6
Number of steps	11
Angular FOV (degrees)	7.5
Step angle (degrees)	9.47
Step time (seconds)	1.84
Ground IFOV at nadir (km diameter)	109.3
Ground IFOV at end of scan	323.1 km cross-track x 178.8 km along-track
Distance between IFOV centers (km along-track)	168.1 km
Swath width	± 1174 km
Time between start of each scan line	25.6 sec
Step and dwell time	1.81 sec
Time difference between the start of each scan and the center of the first dwell period	0.9 sec
Total Channels	4
Channel Frequencies (GHz)	CHs: 1 2 3 4 Frequency: 50.30 53.74 54.96 57.95
Instrument Antenna Systems	MSU-1 and MSU-2
Responsible antennas for each channel	MSU-1 for channels 1 and 2 MSU-2 for channels 3 and 4
Channel Bandwidth (MHz)	200
Blackbody and space views per scan line	1
PRTs on each warm target	2

2.2.2 AMSU-A

As a successor to the MSU instrument, the AMSU-A has 15 discrete frequency channels to measure the Earth scene radiances. At each channel frequency, the antenna beamwidth is a constant of 3.3 degrees (at the half power point). Thirty contiguous scene resolution cells are sampled in a stepped-scan fashion (i.e., the instrument's FOV rotates to a data collection position, stops, collects data, then moves to the next collection position, stops, collects data, etc.) every eight seconds, each scan covering 48.33 degrees on each side of the nadir direction. The AMSU-A instrument starts at earth position 1, then goes

sequentially to earth position 30, then to the cold calibration view position and then to the warm load view position. These scan patterns and geometric resolution translate to a 45 km diameter cell at nadir and a 2,343 km swath width from the 833 km nominal orbital altitude. Detailed AMSU-A instrument characteristics can be found in the NOAA KLM user's guide (Robel et al., 2009)

AMSU-A has two units: A1 and A2; where A1 has two antenna systems, A1-1 and A1-2, and A2 has its own antenna system. Channels 6-7 and 9-15 use A1-1 antenna system, channels 3-5 and 8 use A1-2 antenna system, and channels 1-2 use A2 antenna system. There is a blackbody warm target for each anntana system. Each scan-line contains 30 Earth views, two space views, and two warm target views. The PRTs on each target ranges from 5 to 7, depending on instrument subunits. The averages of the two space views or blackbody views are used to calibrate the 30 Earth views. The warm target temperature is the average of the available good PRTs measurements for each instrument.

Table 2-8 and Table 2-9 summarize the AMSU-A instrument parameters.

Table 2-8 AMSU-A instrument parameters.

Cross-track scan angle (degrees from nadir)	± 48.33
Earth Scene scan time	5.965 seconds
Total Beam Positions	30
Angular FOV (degrees)	3.33
Step angle (degrees)	3.33
Step time (seconds)	0.1988
Ground IFOV at nadir (km diameter)	45km
Swath width	± 1171 km
Time between start of each scan line	8 sec
Step and dwell time	0.1988 sec

Table 2-9 Channel and scanning view parameters for each AMSU-A antenna systems.

Instrument Antenna systems	**A1-1**	**A1-2**	**A2**
Channels	6-7,9-15	3-5, 8	1-2
Earth views per scan line	30	30	30
Blackbody and space views per scan line	2	2	2
PRTs in each warm target	5	5	7

3. Algorithm Description

This section describes the algorithms for the MSU/AMSU-A radiance FCDR as well as the AMSU-A gridded daily brightness temperature FCDR at 80% level of maturity. The MSU/AMSU-A FCDR contains pixel radiances at each scan position in the scan-lines with the original beam directions as well as the limb-corrected beam directions. The gridded daily AMSU-A FCDR products contain daily brightness temperatures on 1°×1° grids. Only the level-1c calibration algorithm and the gridding algorithm are described here.

3.1 Algorithm Overview

The MSU/AMSU-A radiance FCDR is developed using the Integrated Microwave Inter-Calibration Approach (IMICA, formerly known as the simultaneous nadir overpass calibration method, Zou et al., 2006, 2009; Zou and Wang, 2010, 2011). The IMICA method inter-calibrates the level-1c (root-level) MSU and AMSU-A observations by determining offsets and non-linear calibration coefficients from SNO matchups. The IMICA method takes advantages that the SNO matchups do not contain sampling errors such as the diurnal drift errors, so the statistical differences in the SNO matchups represent only the instrument calibration errors in the satellite pairs. The method removed or minimized four types of inter-satellite biases, including constant inter-satellite biases between most satellite pairs, bias drifts on NOAA-16 and certain channels on MetOp-A, solar-heating induced instrument temperature variability in satellite radiances, scene temperature dependency in biases due to inaccurate calibration non-linearity. The inter-calibration resulted in consistent multi-satellite observations with small inter-satellite biases. In addition, SNO analysis method was developed to identify post-launch channel frequency shift from pre-launch specifications or measurements. Using radiative transfer model experiments at the SNO sites, actual channel frequency values were obtained for certain AMSU-A channels. These corrected frequencies are expected to improve accuracies of future applications of these channels in Numerical Weather Prediction (NWP) weather forecasting, climate reanalysis development, as well as TCDR time series.

The gridded daily AMSU-A FCDR products were produced by mapping the AMSU-A level-1c radiance FCDR to the 1°×1° grid. Three algorithms for pixel composing strategies are employed in generating the products:

1. Select only the AMSU-A near nadir pixels (i.e., the scan positions 15 and 16), and average the brightness temperatures of these pixels if more than 1 pixel are accumulated in one grid cell;

2. Among the multiple scan positions (8-23), use the brightness temperature of those closest to the nadir pixels from the AMSU-A radiance FCDR product, i.e., the pixel with minimum viewing zenith angle;

3. Select multiple scan positions (8-23) and average the limb-corrected brightness temperatures of these pixels from the AMSU-A radiance FCDR product.

3.2 Processing Outline

The MSU and AMSU-A radiance FCDR production systems are designed and implemented separately due to differences in instrument characteristics and computer software applied. However, the processing outlines for the two instruments are similar, which are described using the same flowchart as seen below. There is a note for each flowchart to indicate the differences between the MSU and AMSU-A processing systems if such differences exist.

The AMSU-A production system for the daily gridded brightness temperature FCDR requires the radiance FCDR as input, so it is also designed and implemented separately.

3.2.1 Processing Outline of MSU and AMSU-A Radiance FCDR

3.2.1.1 Overall Processing Outline of MSU and AMSU-A Radiance FCDR

The overall processing outline of MSU/AMSU-A radiance FCDR algorithm is summarized in Figure 3-1. The current MSU/AMSU-A FCDR algorithm is implemented at orbital-level, with one inter-calibrated level-1c file corresponding to one MSU/AMSU-A level-1b file. In an orbit, raw counts data of the Earth views are converted to radiances scan-line by scan-line. Limb-corrected radiances are also generated to adjust off-nadir observations to nadir equivalent observations.

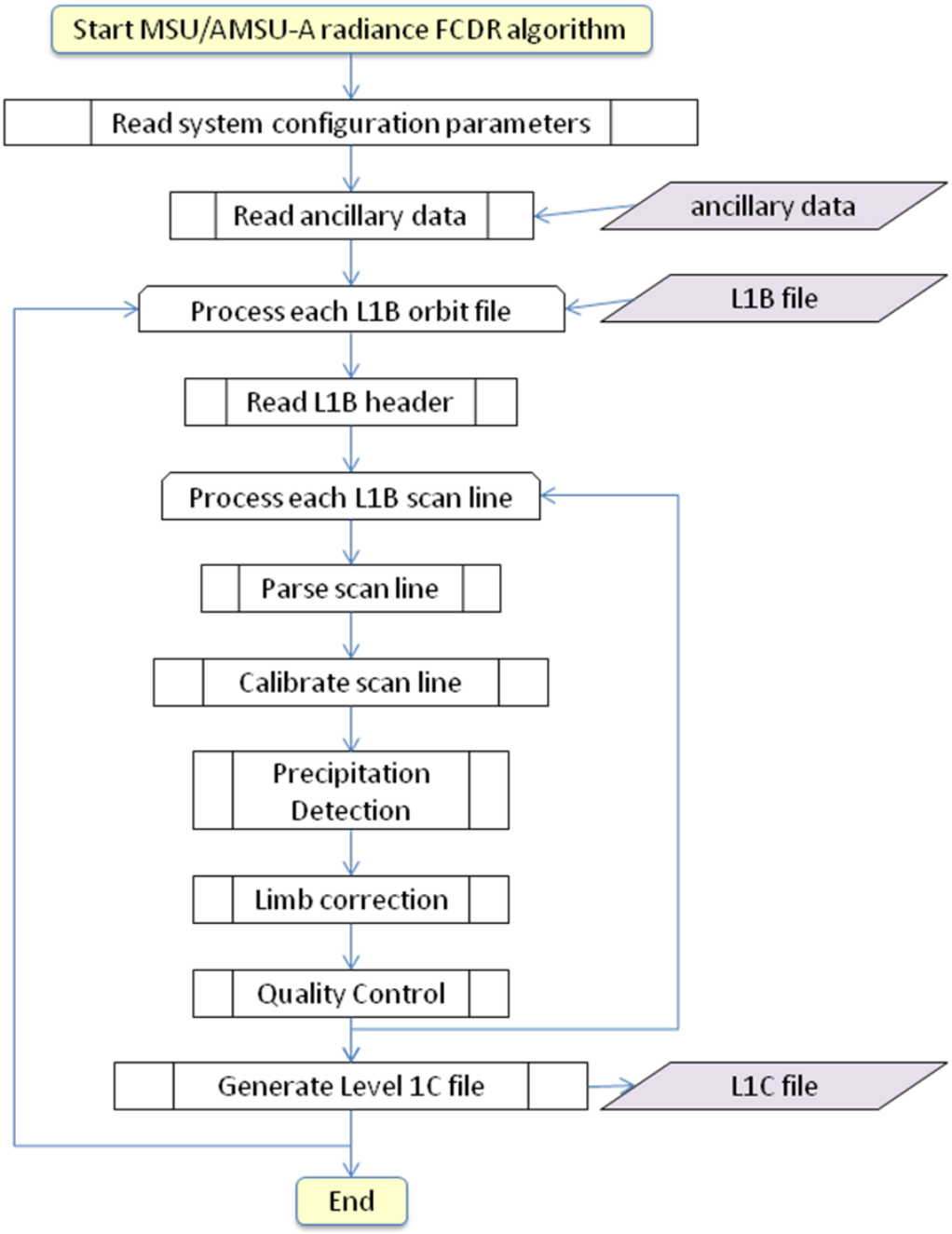

Figure 3-1 High level flowchart of the MSU/AMSU-A FCDR algorithm illustrating the main processing section.

3.2.1.2 System Configuration for the MSU/AMSU-A Radiance FCDR Processing

The processing starts with system configuration, including defining satellite names, level-1b input and level-1c output directories, ancillary data directories, and calibration methodologies (Figure 3-2). In addition to the IMICA inter-calibration method,

the FCDR production system supports two other calibration methods: the NOAA pre-launch calibration and linear calibration. The AMSU-A FCDR generation system supports parallel processing to address the large data volume issue in AMSU-A. System operators should first define the maximum number of the level-1b files that can be simultaneously processed by the computer based on the computer hardware environment.

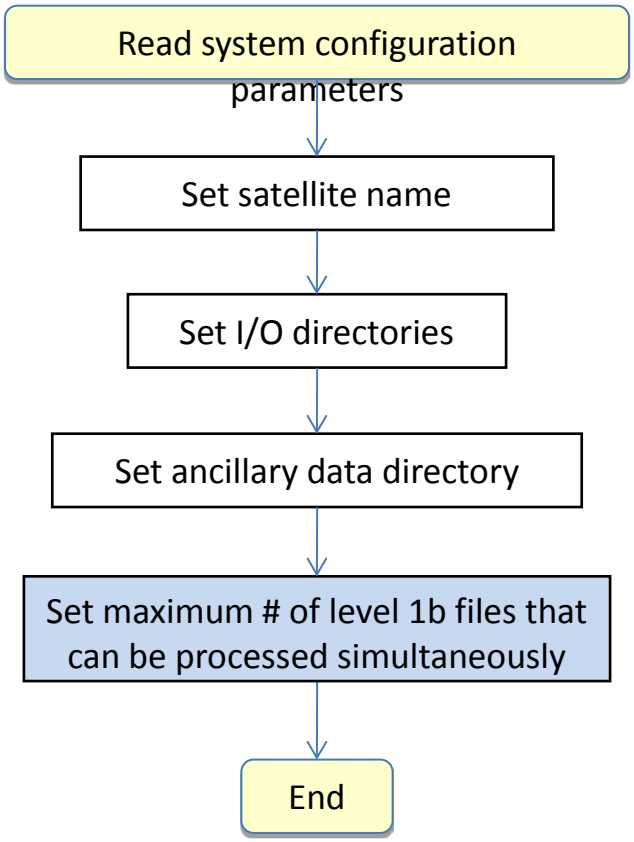

Figure 3-2 Input parameter processing flowchart for the MSU/AMSU-A FCDR. The box with light blue background is for AMUS-A only. Note: the MSU code doesn't support parallel processing.

3.2.1.3 Preparing Ancillary Data

Several ancillary data are required to generate level-1c recalibrated files from level-1b files. These ancillary data consist of land fraction, IMICA calibration coefficients, and limb correction coefficients. Figure 3-3 shows the flowchart for preparing the ancillary data. Note that the antenna pattern correction coefficients are not available for the MSU observations, so the 'read antenna pattern correction coefficients' component should be removed for the MSU processing system. In addition, the AMSU-A antenna pattern correction is not currently used for all satellites.

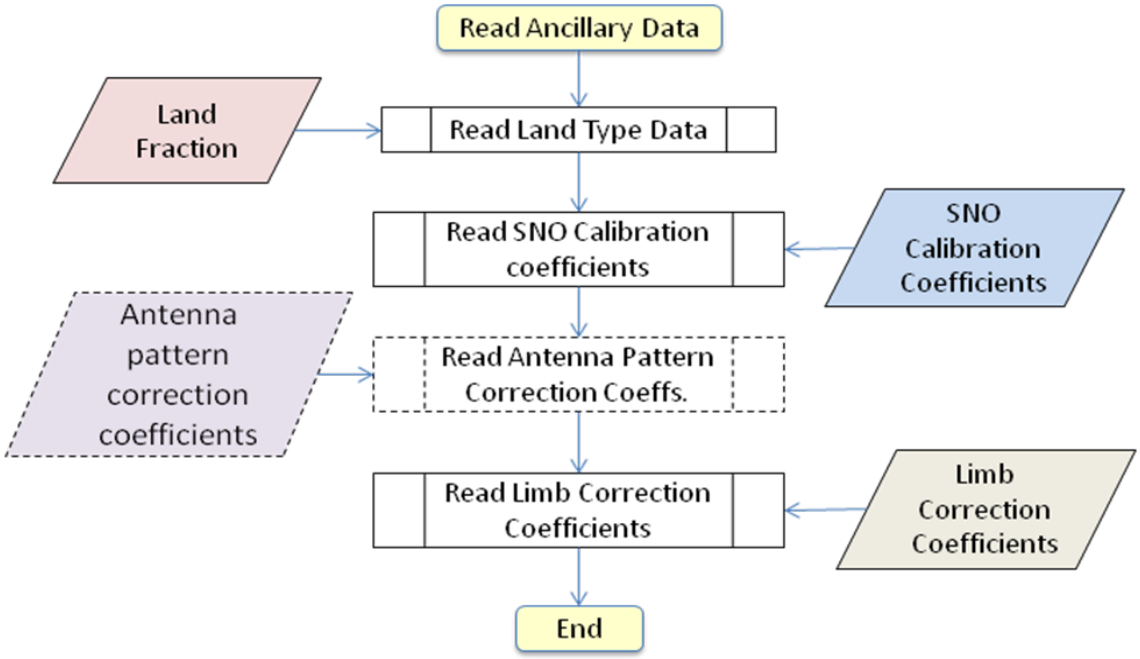

Figure 3-3 AMSU-A FCDR flowchart for preparing the ancillary data. There is no antenna pattern correction for the MSU instrument; therefore, the 'read antenna pattern correction coefficients' component should be removed when the flowchart is used for the MSU processing system.

3.2.1.4 Processing Level-1b Header Record

The header record in each MSU/AMSU-A level-1b file contains orbit-wide information for the subsequent calibration process. These information includes data creation site ID, satellite/instrument ID, observation time, number of data record, instrument reference temperature, warm target and cold space correction factors (AMSU-A only), central wave numbers (AMSU-A only), coefficients for calculating nonlinear parameters, coefficients for converting raw counts of varies instrument temperature readings to the actual instrument temperatures, etc. Figure 3-4 illustrates how AMSU-A header record is processed in the FCDR processing system. The MSU systems have less parameters than the AMSU-A for processing.

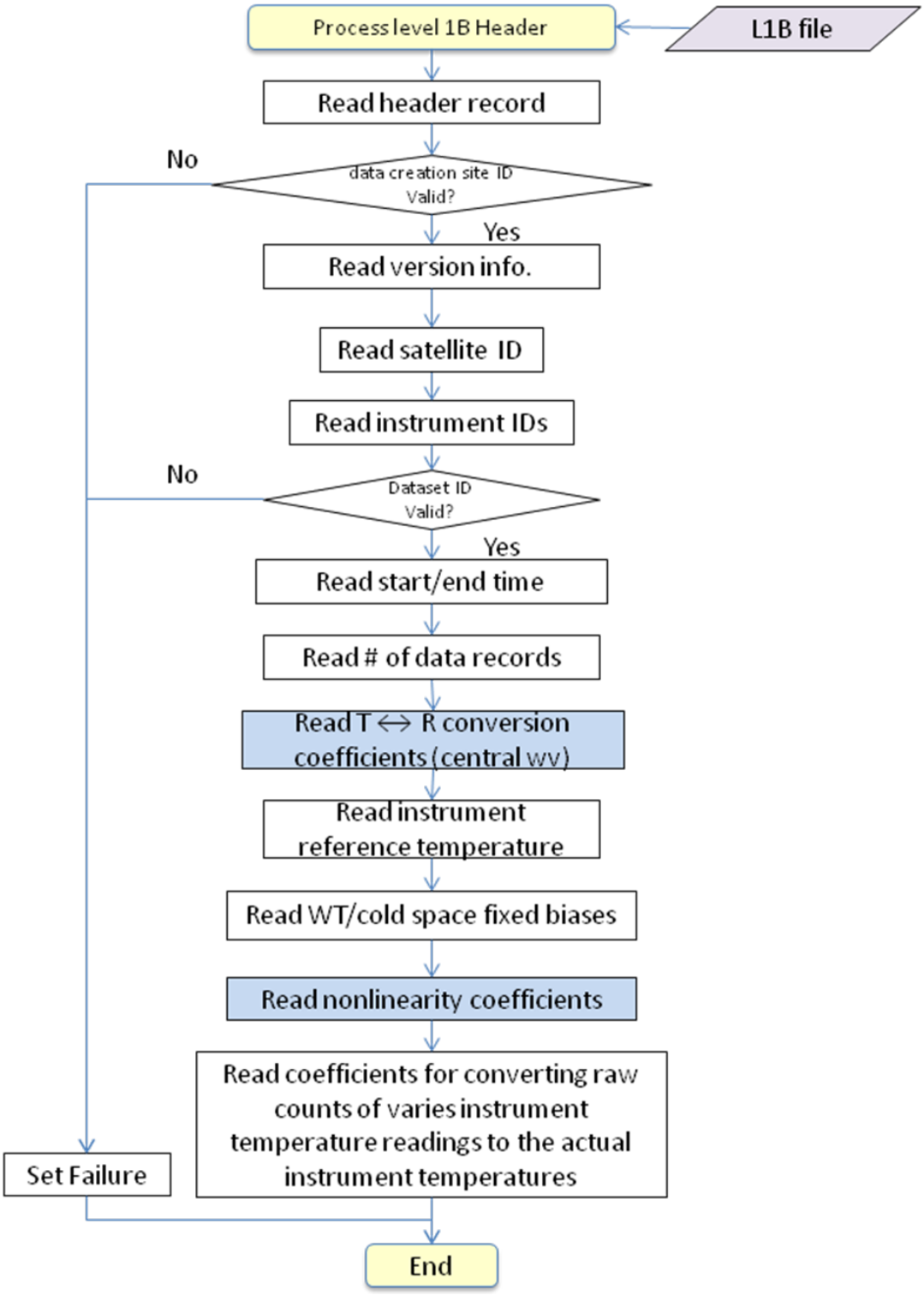

Figure 3-4 Flowchart for processing MSU/AMSU-A level 1B header record (steps with light blue background are for AMSU-A only).

3.2.1.5 Preprocessing Level-1b Scan Line

Each level-1b file is decoded line by line before generating a level-1c scan line. Figure 3-5 shows flowchart for preprocessing each AMSU-A level-1b data record.

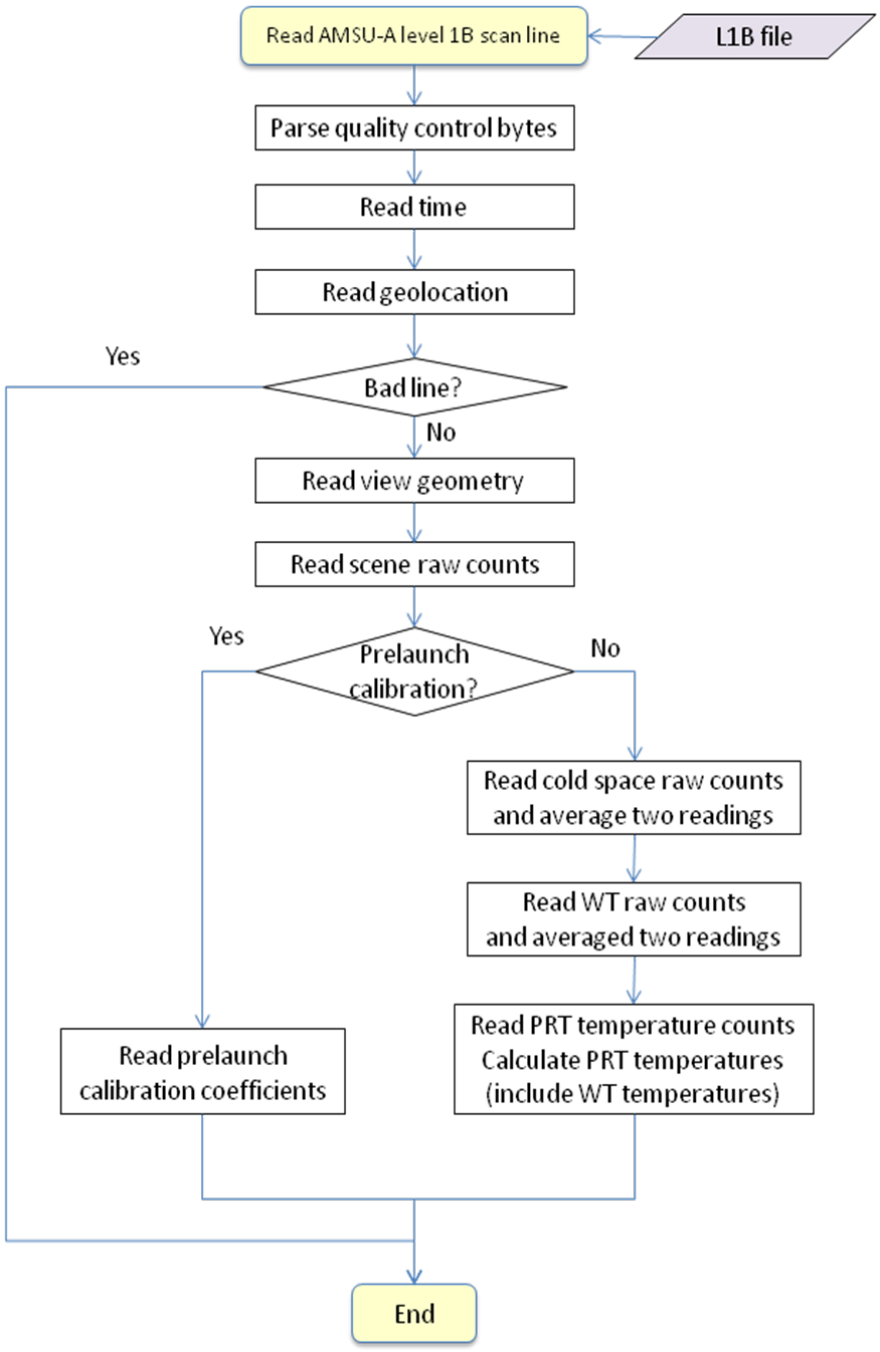

Figure 3-5 Flowchart of parse MSU/AMSU-A FCDR level-1b scan line.

3.2.1.6 Level-1c Calibration

Figure 3-6 shows the flowchart of the level 1c calibration process for converting the Earth scene raw counts to radiances. There are three calibration methodologies in the processing system: IMICA, pre-launch, and linear calibrations. The FCDR outputs contain calibrated radiances from both the IMICA and pre-launch calibrations for channels with available SNO calibration coefficients (MSU channels 2-4, AMSU-A channels 4-14). For channels without the SNO calibration coefficients (MSU channel 1, AMSU-A channels 1-3, 15), only pre-launch operational calibration is conducted. The linear calibration is optional in the processing system for research purposes –its output is not part of the FCDR dataset.

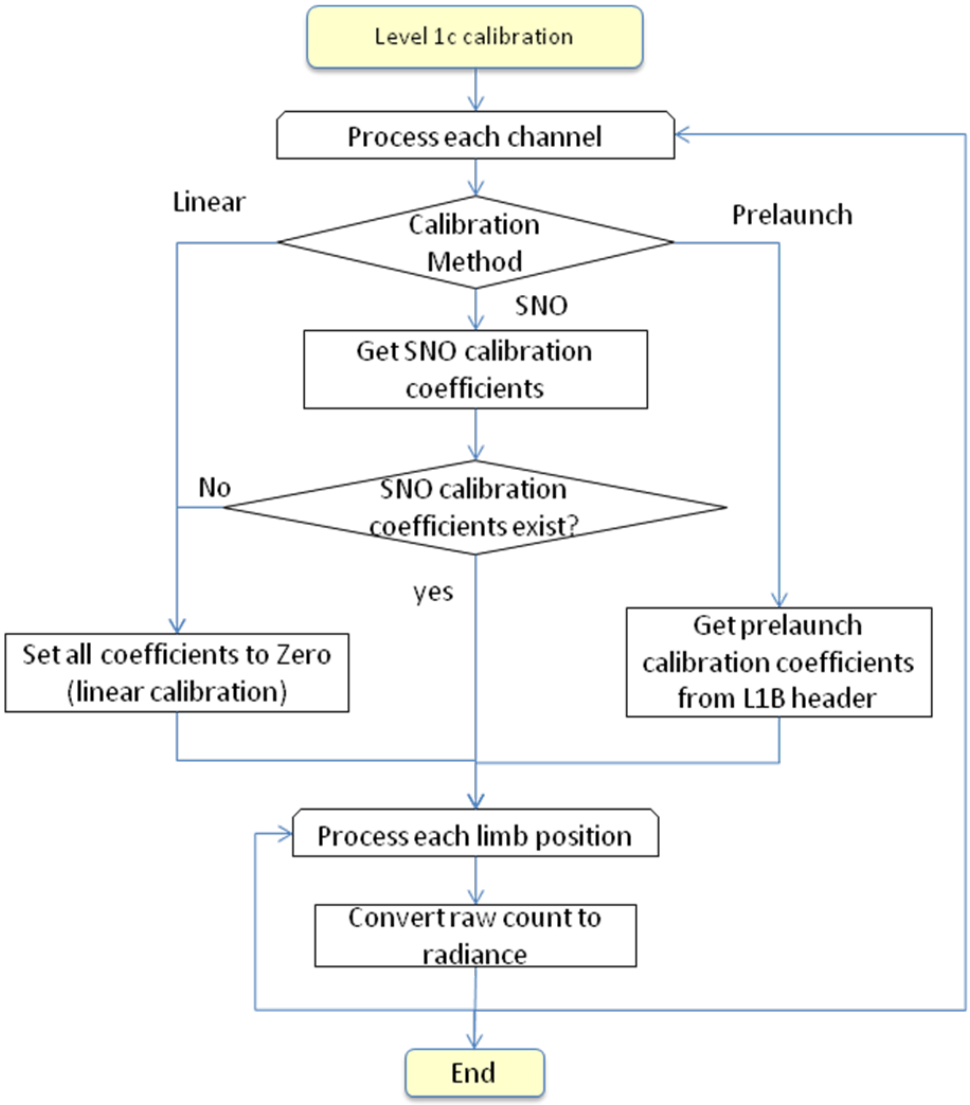

Figure 3-6 Flowchart of the MSU/AMSU-A level-1c calibration.

3.2.2 Processing Outline of the AMSU-A Daily Gridded Brightness Temperature FCDR

3.2.2.1 Overall Processing Outline of AMSU-A Gridded FCDR Processing

The overall processing outline of the algorithm for gridded daily AMSU-A FCDR products is illustrated in Figure 3-7. Details for each step are described in the following sections.

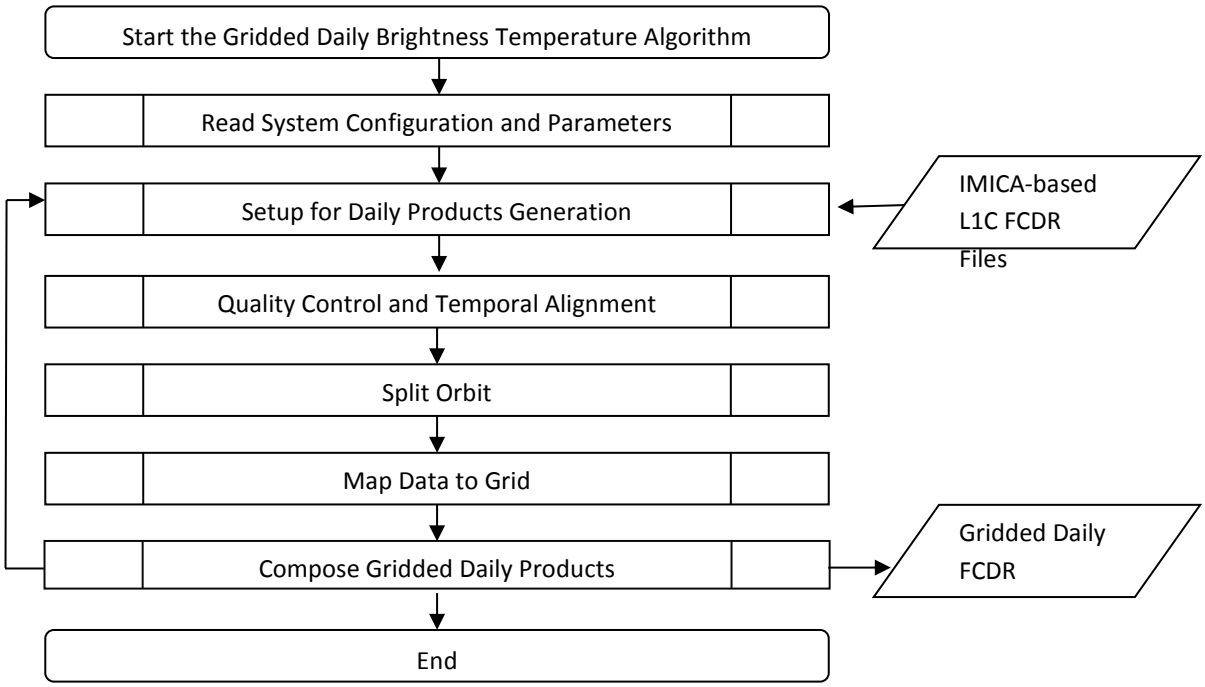

Figure 3-7 Diagram for generating AMSU-A gridded daily brightness temperature FCDR.

3.2.2.2 System Configuration for AMSU-A Gridded FCDR Processing

The processing starts with system configuration, including list of satellite names, level-1c input directories, output directories, ancillary data directories, and time ranges. These are shown in figure 3-8.

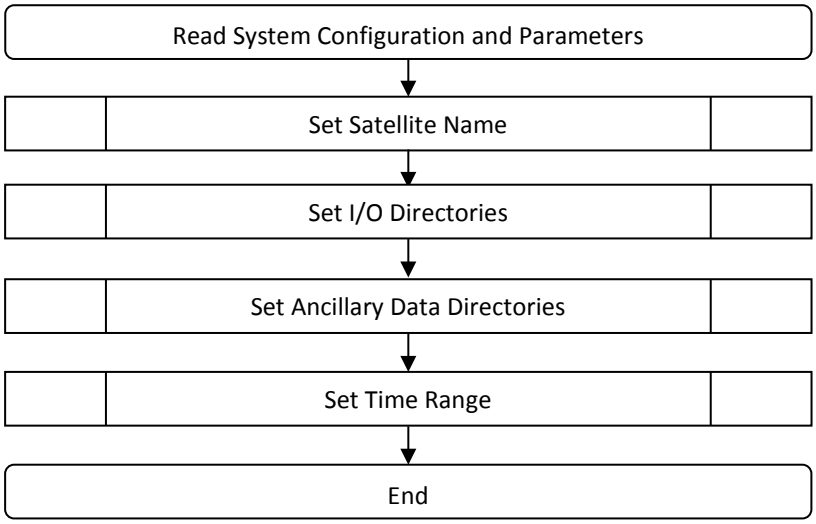

Figure 3-8 Diagram of system configuration for generating AMSU-A daily gridded brightness

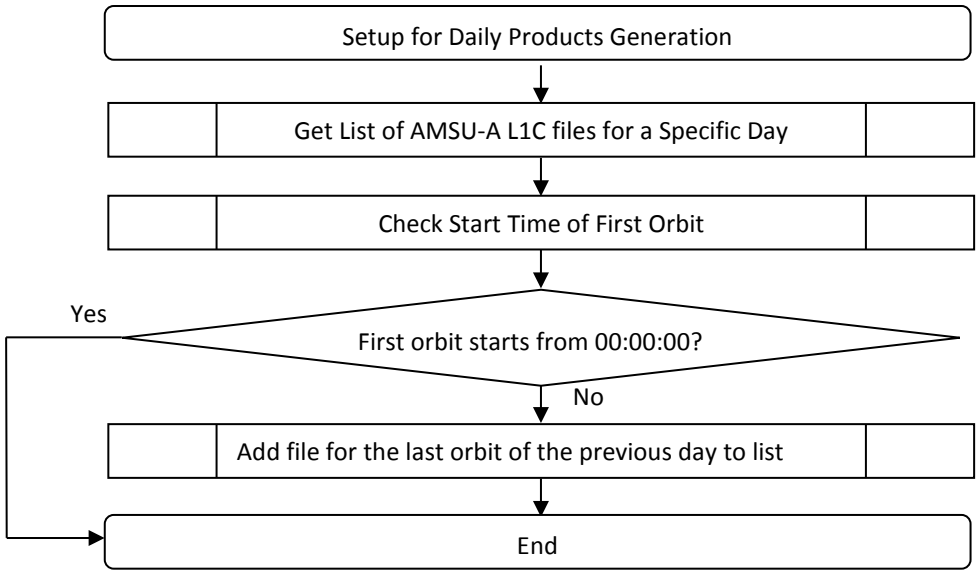

Figure 3-9 Diagram for AMSU-A daily gridded FCDR products generation setup.

3.2.2.3 Setups for AMSU-A Daily Gridded FCDR Products Generation

The gridded AMSU-A FCDR products are processed at daily level. For each day, a list of the IMICA-based AMSU-A level-1c FCDR files is determined first. The IMICA AMSU-A Level 1c FCDR files are processed at orbital level and named with information including year, month, day, starting hour and minute, and ending hour and minute. For a specific day,

the required level 1c files for the daily gridded data products include all level-1c files for that day, and may also include level 1c files of the last orbit in the previous day. As illustrated in figure 3-9, this step will check the temporal coverage of each level 1c file, and create a list of available level 1c FCDR files for the specific day for gridded FCDR generation.

3.2.2.4 Quality Control and Temporal Alignment

After the list of the IMICA AMSU-A level 1c files for a specific day is determined from previous step, the system will read the files into memory according to the order of starting time to check data quality of each scan and determine valid scans and pixels for daily products generation.

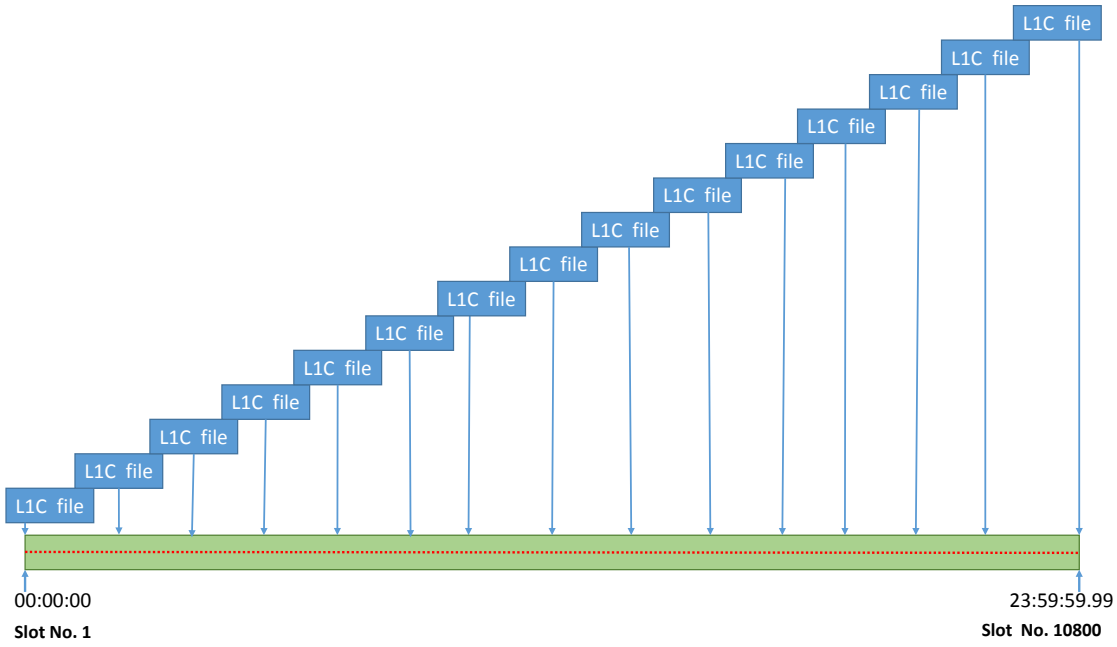

Figure 3-10 Diagram of temporal alignment of orbital level 1c data.

The level 1c files may overlap over time, having invalid data or missing scans, it is necessary to remove repetitive and invalid data before mapping them into grid. Quality control aims to check missing data and remove invalid values. Temporal alignment aims to remove repetitive scans among multiple level 1c files. Figure 3-10 illustrated the process of temporal alignment. For AMSU-A, since the time between the start of each scan is 8 seconds, the total number of scans for each day is 10800. For each scan in the level 1c files, a check is first conducted to see if data is valid. If data is invalid, skip it. If data is valid, another check on the corresponding time is conducted to see if valid data for that time has been marked as available. If already available, skip this repetitive scan; otherwise, select this scan for the corresponding time and mark flag as valid. The quality control and temporal alignment steps result in a total of 10800 scans for each day (may contain invalid scans and pixels), including time, geolocations, view zenith angles, brightness temperature of each channel, as well as flags to indicate quality of each scan.

3.2.2.5 Splitting Orbit

Daily gridded AMSU-A FCDR data are generated for ascending orbits and descending orbits separately. Geo-location at nadir pixels (scan positions 15 and 16) are used to determine the flight directions of a satellite and to split the ascending and descending orbits. For each scan, if the nadir latitude is larger than the previous scan, it is marked as the ascending orbits; otherwise, it is marked as the descending orbits. In case that the geo-location of pixels in previous scans is invalid, a comparison to the next scan is used to determine the satellite flight direction.

3.2.2.6 Mapping Data to Grid

The grid has a resolution of 1°latitude by 1° longitude, with longitude from -179.5° to 179.5° and latitude from 89.5° to -89.5°. So the data grid has 180 rows from 0 to 179 and 360 columns from 0 to 359. After the previous steps for quality control and temporal alignment, 10800 scans are composed and marked with ascending/descending flags for each day. Each scan has 30 pixels, however, only pixels from scan positions 8 to 23 were used in the daily gridded products, since limb-adjustments for these scan positions resulted in the smallest off-nadir biases. For each pixel, its row and column on the 1°×1° grid are determined from the following equations:

$$\boldsymbol{row} = \boldsymbol{floor}(\mathbf{90} - \boldsymbol{latitude}) \qquad (3\text{-}1)$$

$$\boldsymbol{col} = \boldsymbol{floor}(\boldsymbol{longitude} + \mathbf{180}) \qquad (3\text{-}2)$$

Then, all pixels for one day are mapped into the grid according to row and column calculated from the above equations for spatial composition.

3.2.2.7 Generating AMSU-A Daily Gridded FCDR products

Three daily gridded AMSU-A FCDR products were generated according to the three different methods for pixel composition: 1) near-nadir only; 2) minimum view zenith angle (closest to nadir); and 3) means of all the pixels for scan positions (8-23). Detailed approaches for these compositions are described in the Theoretical Description of the algorithm.

3.3 Algorithm Input

This section describes the attributes of all input data used by the algorithm, including primary sensor data and ancillary data.

3.3.1 Primary Sensor Data

Table 3-1 lists the primary sensor data (data directly available from the MSU/AMSU-A level-1b files used by the MSU/AMSU-A FCDR algorithm, including raw counts for the Earth view, warm target view, and cold space view; warm target temperatures, geo-location information, and sensor quality flags).

Table 3-1 MSU/AMSU-A primary sensor data at pixel level. The dimension 'xsize' is the pixel number per scan-line (11 for MSU and 30 for AMSU-A) and 'ysize' is the total scan-line number in an orbital file.

Name	Type	Description	Dimension
Earth Scene Raw Counts	Input	Earth Scene raw counts for atmospheric temperature channels (MSU channels 1-4; AMSU-A channels 1-15)	pixel (xsize, ysize)
Cold Space Raw Counts	Input	Cold Space raw counts corresponding to each MSU/AMSU-A atmospheric temperature channel	pixel (xsize, ysize)
Warm target raw Counts	Input	Warm target raw counts corresponding to each MSU/AMSU-A atmospheric temperature channel	pixel (xsize, ysize)
Warm target temperatures	Input	Warm target temperatures, average of the available good PRT readings	pixel (xsize, ysize)
Latitude	Input	Pixel center latitude	pixel (xsize, ysize)
Longitude	Input	Pixel center longitude	pixel (xsize, ysize)
QC flags	Input	quality control flags from level-1b data	pixel (xsize, ysize)
Pre-launch calibration coefficients	Input	Pre-launch calibration coefficients	

The actual sensor inputs are different for different calibration methods. The IMICA and linear calibrations require the raw counts data for the Earth view, cold space view, and warm target view, as well as the warm target temperatures. The NOAA pre-launch calibration takes a simplified form where the Earth scene radiance is polynomial proportional to the Earth view counts with the raw counts and temperatures for the calibration targets as well as the nonlinear coefficients of the original calibration equation being absorbed in the calibration coefficients of the polynomial equation. See Section 3.4 for a theoretical description of the IMICA calibration method and the NOAA KLM Users Guide (Robel et al., 2009) for the NOAA pre-launch calibration method.

The primary input data for the gridding algorithm are the IMICA calibrated AMSU-A L1C radiance FCDR, i.e. the output of the AMSU-A L1C FCDR algorithm.

3.3.2 Ancillary Data

The calibration algorithm requires three types of ancillary data:

i. SNO calibration coefficients (Table 3.2 for MSU and Table 3.3 for AMSU-A);

ii. Limb correction coefficients (available in the FCDR generation system package);

iii. Land mask data [land or ocean, where a pixel is considered as ocean (land) if the ocean percentage in the pixel is greater (smaller) than 50%]

3.3.3 Derived Data

Not Applicable.

3.3.4 Forward Models

Not Applicable.

3.4 Theoretical Description

This section describes the physics for the development of consistent MSU/AMSU radiance FCDR using the IMICA inter-calibration algorithm, and the development of AMSU-A daily gridded brightness temperature FCDR. There are three parts in the algorithm:

i. obtain the calibration coefficients using the regression equation 1-2

ii. calculate consistent radiance FCDR data using the calibration equation 1-1

iii. grid the AMSU-A radiance FCDR

The second part of calculation is straightforward given the sensor data from the level-1b files and the ancillary data described in Section 3.3.2. It is similar to the operational calibration except that the latter uses calibration coefficients determined from laboratory chamber test experiments (e.g., Mo, 2006) while the former uses calibration coefficients determined by the SNO regressions of Equation 1-2. This part of the algorithm mainly involves data processing similar to operational calibration and its physical basis has been well established in documents describing the operational level-1b data processing (e.g., Mo, 2006; Robel et al., 2009, and related references). However, results of the part (i) algorithm are a prerequisite for deriving the radiance FCDR using the part (ii) algorithm and the part (i) algorithm itself involves knowledge and understanding of the calibration errors, SNO regressions, and a comprehensive end-to-end calibration process to determine the calibration coefficients as listed in Tables 3-2 and 3-3. In the following sections, part (ii) algorithm is described first (Section 3.4.1) followed by a description of the part (i) algorithm (Section 3.4.2). Part (i) can be skipped if one is only interested in generating the final radiance FCDR products using the given calibration coefficients.

The part (iii) algorithm for mapping AMSU-A level-1c FCDR data to grid is straightforward in theory. However, due to repetition of swatch data in level 1C FCDR and data quality control, special processing is required to ensure gridding accuracy. Detailed description on the gridding approach is thus provided.

3.4.1 Physical and Mathematical Description

The MSU and AMSU instruments use an on-board calibration method that includes two calibration targets as its end point references: the cosmic space cold target and an onboard blackbody warm target. The cold space has a temperature of 2.73 K, and the warm target temperature is measured by the platinum resistance thermometers (PRT) embedded in the blackbody target. In each scan cycle, the MSU/AMSU-A looked at these targets as well as the earth, and the signals in the form of electric voltage were converted to digital counts through an analog-to-digital converter. These digital counts were output as raw observations. A calibration equation, also known as radiometer transfer function, is used to convert the raw counts observations to the radiances using the two calibration targets.

The level-1c calibration equation to generate the MSU/AMSU-A FCDR is written as (Zou et al., 2006, 2009):

$$R = R_L - \delta R + \mu Z \qquad (3\text{-}3)$$

where R is the earth scene radiance, $R_L = R_c + S(C_e - C_c)$, representing the dominant linear response, and $Z = S^2(C_e - C_c)(C_e - C_w)$ is a nonlinear response. C represents the raw counts data of the satellite observations and $S = \frac{R_w - R_c}{C_w - C_c}$ is the slope determined by the two calibration targets. The subscripts *e, w* and *c* refer to the earth-view, onboard blackbody warm target view, and cold space view, respectively; δR represents a radiance calibration offset; and μ is a nonlinear coefficient. A schematic viewing of this calibration process is illustrated in Figure 3-11.

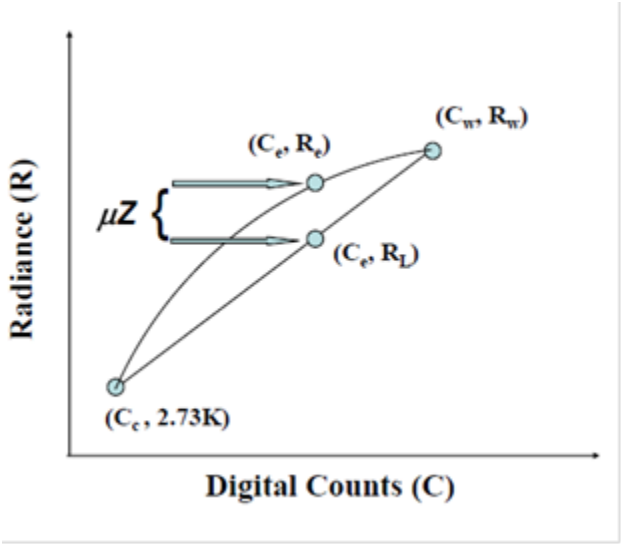

Figure 3-11 Schematic viewing the calibration principle of the MSU/AMSU instruments. Symbols used in the plot are defined in the main text.

In Equation 3-3, the cold space radiance Rc is set to be the value that corresponds to a brightness temperature of 4.73 K for all scan lines of the MSU and AMSU observations. This value includes the cold-space temperature of 2.73 K plus an increase of about 2 K owing to the antenna side-lobe radiation. The algorithms described in (Kidwell, 1998) for MSU and in (Robel et al., 2009) for AMSU are used to compute R_w. Once the calibration offset, δR, and the nonlinear coefficient, μ, are known, radiance is computed through Equation 3-3 and the brightness temperature, T_b, is then computed using the Planck function.

Equation 3-3 or 1-1 is a modified version of the algorithm used by NOAA for operational generation of the level-1c products, where δR was assumed to be zero and the non-linear coefficient μ was determined from pre-launch laboratory tests (Mo, 1996). These coefficients have been converted to polynomial coefficients with respect to scene counts (Robel et al., 2009) and then stored in AMSU-A level 1b files. Radiances calculated using coefficients in AMSU-A level 1b files are hence referred to as the operational calibration. However, because this procedure was repeated for each AMSU-A instrument independently, it was not designed to correct for residual biases between satellites.

In the inter-satellite calibration described in this document, the offset δR in Equation 3-1 allows for removal of inter-satellite differences. In addition, the calibration coefficients, δR and μ, were determined using SNO matchups. There is another difference from the operational calibration. In specific, the raw counts values of the calibration targets in Equation 3-1 were averages over 7 adjacent scan lines in the operational calibration (Mo, 1996). However, in the IMICA inter-satellite calibration, target counts values of a single scan line were used to calibrate each Earth scene observation in that scan line. This change was made because SNOs are collected for individual near nadir footprints. When deriving calibration coefficients from SNOs, target observations closest to the SNO footprints, which are those from the same scan lines of the SNO events, are used to eliminate potential non-simultaneous errors. Limited experiments indicate that this change may increase the noise in the level-1c radiances by 2% compared to those using the original method of averaging adjacent scan lines. This small extra noise is not expected to affect the quality of the resulting level-1c radiances. However, if future evidence suggests that this will cause large errors in the weather and climate reanalysis data assimilations, we will use the operational algorithm for target counts calculation but with SNO calibration coefficients applied.

Quality control procedure in the operational calibration is used in the SNO inter-calibration to deal with missing calibration information, instrument anomalies, and bad scan lines.

3.4.2 Inter-Satellite Calibration Methodology

Developing consistent radiance FCDR mainly involves minimizing inter-satellite radiance biases between satellite pairs through an inter-calibration process. An IMICA inter-calibration methodology is developed at NOAA/NESDIS (Zou et al., 2006, 2009) to remove or minimize calibration errors that were not well resolved by the pre-launch

operational calibration. These errors include constant inter-satellite biases between most satellite pairs, bias drifts in certain satellite channels, solar-heating induced instrument temperature variability in radiances, scene temperature dependency in biases due to inaccurate calibration non-linearity, and biases owing to channel frequency shift from its prelaunch measurement in certain satellite channels. A detailed description on the origin and nature of these biases can be found in Zou and Wang (2011).

Optimal calibration coefficients, δR and μ, were determined from SNO repressions to remove the first four types of biases. The SNO matchups, occurring mostly over the Polar Region around 80°S and 80°N, were accumulated using Cao et al.'s (2004) algorithm. The ground distance and time criteria for the SNO matchups were respectively set to be 111 km and 100 seconds for the MSU satellites for TIROS-N through NOAA-14 and 45 km and 50 seconds for the AMSU-A satellites for NOAA-15 through NOAA-18, and MetOp-A. The SNO matchups do not contain sampling errors such as the diurnal drift errors. Therefore, the statistical differences in the SNO matchups represent instrument calibration errors in the satellite pairs.

Applying the calibration Equation 3-1 to the SNO matchups between two satellites, represented by *k* and *j*, a radiance error between them is derived as,

$$\Delta R = \Delta R_L - \Delta \delta R + \mu_k Z_k - \mu_j Z_j + E \qquad (3\text{-}4)$$

Where $\Delta R_L = R_{L,k} - R_{L,j}$ and $\Delta \delta R = \delta R_k - \delta R_j$. E is a residual term related to the spatial and time differences between the satellites *k* and *j* and is ignored. In Equation 3-4, ΔR_L, Z_k and Z_j are a function of the measurements while $\Delta \delta R$, μ_k, and μ_j are unknown coefficients. Regression methods are used to solve for these coefficients from the SNOs in which the summation of $(\Delta R)^2$ is minimized. Optimum values of the three parameters, $\Delta \delta R$, the difference between μ_k and μ_j, (μ_k-μ_j), and the absolute values of μ_k or μ_j, determined from the regressions remove three different type of errors: the mean radiance bias in the satellite pair, the scene temperature dependency in biases, and the solar-heating induced instrument temperature variability in the radiances.

Figure 3-12 shows an example of the brightness temperature differences in the SNO matchups between NOAA-10 and NOAA-11 before and after applications of the SNO regression coefficients in the calibration Equation 3-3. In specific, Figure 3-12a shows SNO scatter plot between NOAA-10 and NOAA-11 of the linear calibrated data form MSU channel 2. Inter-satellite bias of -0.3 K and scene temperature dependency in the biases are clearly seen in the plot. These biases occur due to inaccurate calibration offsets and nonlinearity. These scene temperature dependent biases can be quantified by the slope of the SNO scatter plot between the two satellites. This slope (0.0206) results in about 0.3 K biases between NOAA-11 and NOAA-10 for a temperature range of 150 K (from 200 to 250K). This scene temperature dependency causes the inter-satellite biases to depend on latitude and season.

Figure 3-12b shows the same SNO scatter plot but with brightness temperatures being calculated from applying the optimum calibration coefficients determined from the

SNO regressions. It is clearly seen that the SNO determined calibration coefficients have removed the mean inter-satellite biases in the satellite pairs and significantly reduced the scene temperature dependency in the biases.

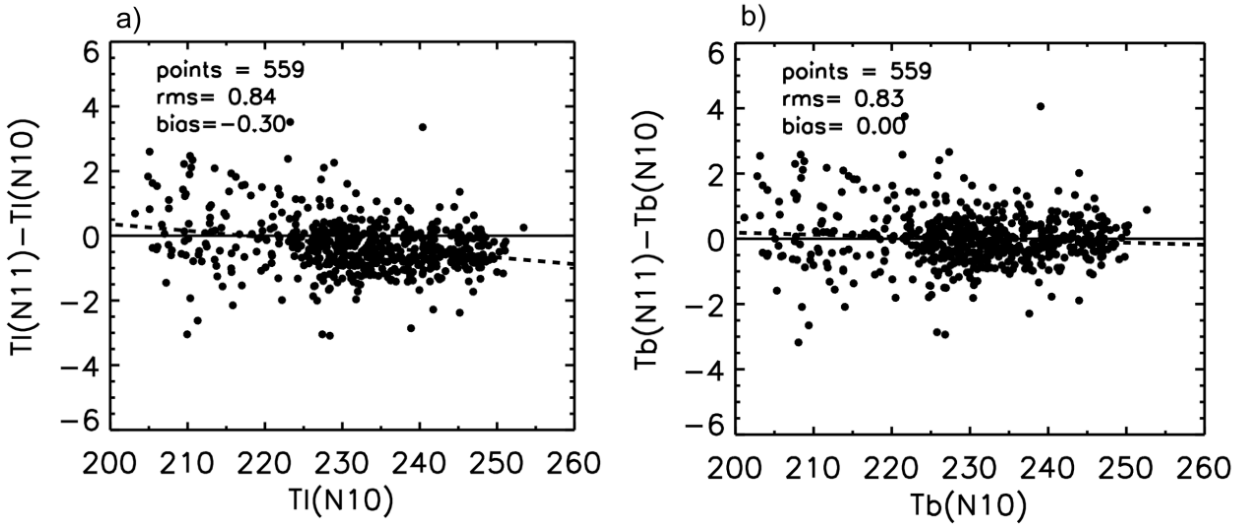

Figure 3-12 (a) SNO scatter plot between T_b(N10) and δT_b = T_b(N11)-T_b(N10), showing scene temperature dependent biases when T_b (represented by T_L) is obtained by linear calibration equation. The regression linear fitting (dashed lines) is expressed as ΔT_L = 4.491–0.0206×T_L(N10); (b) Same as (a) but for SNO calibrated data between T_b(N10) and δT_b = T_b(N11)-T_b(N10). The regression linear fitting (dashed lines) is expressed as ΔT_b = 1.42–0.00615×T_b(N10) (Plots from Zou et al. 2006).

Note that optimum differences of the calibration coefficients, $\Delta\delta R$ and (μ_k-μ_j), are sufficient to remove the inter-satellite biases and their scene temperature dependency in Figure 3-12. Thus the absolute values of the calibration coefficients must be determined using other information. For this purpose, one of the satellites in the pair (k and j) should be selected as a reference satellite. For this reference satellite, the calibration offset shall be determined from an absolute calibration effort or validation against observations from other reference observations. Since such references do not exist, the offset of the reference satellite is arbitrarily chosen to be zero.

The absolute value of the nonlinear coefficient of the reference satellite is determined using the requirement that instrument temperature dependency in the radiances must be minimal for the satellite pair. Using NOAA-15 and NOAA-16 satellite pair as an example, Figure 3-13 visually demonstrates how absolute values of optimum calibration coefficients were obtained from the SNO calibration procedure. In the plot, the quadratic curves in each panel respectively represent calibration equations for NOAA-15 and NOAA-16 for a specific combination of the non-linear coefficients, μ_{N15} and μ_{N16}, with their differences, μ_{N15}-μ_{N16}, determined by their SNO matchups. Also shown in each panel is their SNO T_b difference time series corresponding to the calibration curves within the panel. Changing the calibration coefficient, μ_{N15}, of the reference satellite also changes μ_{N16} due to their SNO constraint. These changes resulted in graduate changes in magnitude

from Figures 3-13a to 3-13d of the solar-heating induced instrument temperature variability in their SNO T_b difference time series. Only a unique combination of the calibration coefficients, μ_{N15} and $\mu_{N16,}$ can minimize the instrument temperature variability (Figure 3-13c). For a more detailed description of the procedure, the readers are referred to Zou et al**.** (2006, 2009) and Zou and Wang (2011).

Based on these SNO regression characteristics, a sequential procedure (Zou et al., 2006, 2009) was developed to obtain calibration coefficients for the MSU/AMSU-A instruments for all satellites. Following this method, a reference satellite is selected and its calibration coefficients, δR and μ, are assumed to be known temporarily. Then calibration coefficients of all other satellites are determined sequentially (one by one) from regressions of the SNO matchups between satellite pairs, starting from the satellite closest to the reference satellite. For the MSU observations, NOAA-10 was selected to be the reference satellite. For AMSU-A observations, the reference satellites were selected to be NOAA-18 for channel 6 and NOAA-15 for all other channels. The calibration offset δR was arbitrarily set to be zero for the reference satellite since it does not affect the climate variability and trends. The sequential procedure actually reduces the problem to the determination of the nonlinear coefficient of the reference satellite; since once it is known, calibration coefficients of all other satellites are solved from the SNOs.

The nonlinear coefficient of the reference satellite was determined by the requirement that the averaged solar-heating induced temperature variability in the radiances for all satellite pairs should be minimal. To meet this requirement, a series of sensitivity experiments was conducted in which the nonlinear coefficient of the reference satellite was selected at different values within a reasonable range. For each given value, a set of calibration coefficients for all other satellites were obtained sequentially from regressions of the SNO matchups. For each set of calibration coefficients, level-1c radiances were generated for all satellites and the solar-heating induced temperature variability were examined in the global ocean mean time series. The final determination of the nonlinear coefficient was made when the average of this variability is minimal for all satellites. This approach generates a set of level-1c radiances that does not depend on the initial selection of the reference satellite. Figure 3-14 shows the flowchart for the above described sequential procedure.

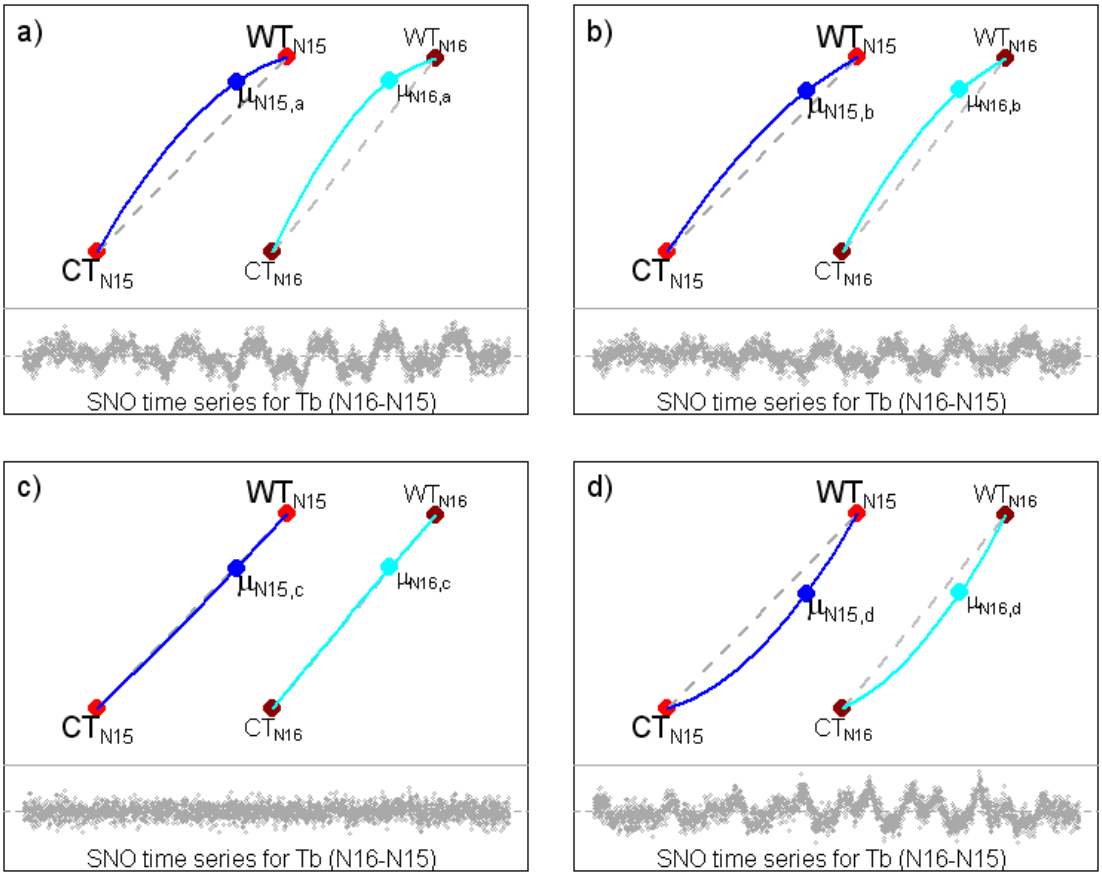

Figure 3-13 Schematic plots showing how sun-heating-induced instrument temperature signals in radiances were removed by appropriate combination of the non-linear calibration coefficients between two satellites. In each panel, the top two quadratic curves respectively represent calibration equations for NOAA-15 and NOAA-16 corresponding to different values of non-linear coefficients μ_{N15} and $\mu_{N16,}$ where the horizontal coordinate represent the raw counts and the vertical coordinate represents the radiance. Symbols CT and WT stand for cold and warm targets, respectively. The lower time series are SNO T_b differences for channel 7 between the two satellites (NOAA-16 minus NOAA-15) with horizontal coordinates being the time and vertical coordinates being the T_b differences. Note the graduate changing of the sun-heating-induced instrument temperature variability in the SNO time series for panels (a), (b), (c) and (d). Also note only at a unique combination of μ_{N15} and μ_{N16} (panel c) that this instrument temperature variability is mostly removed.

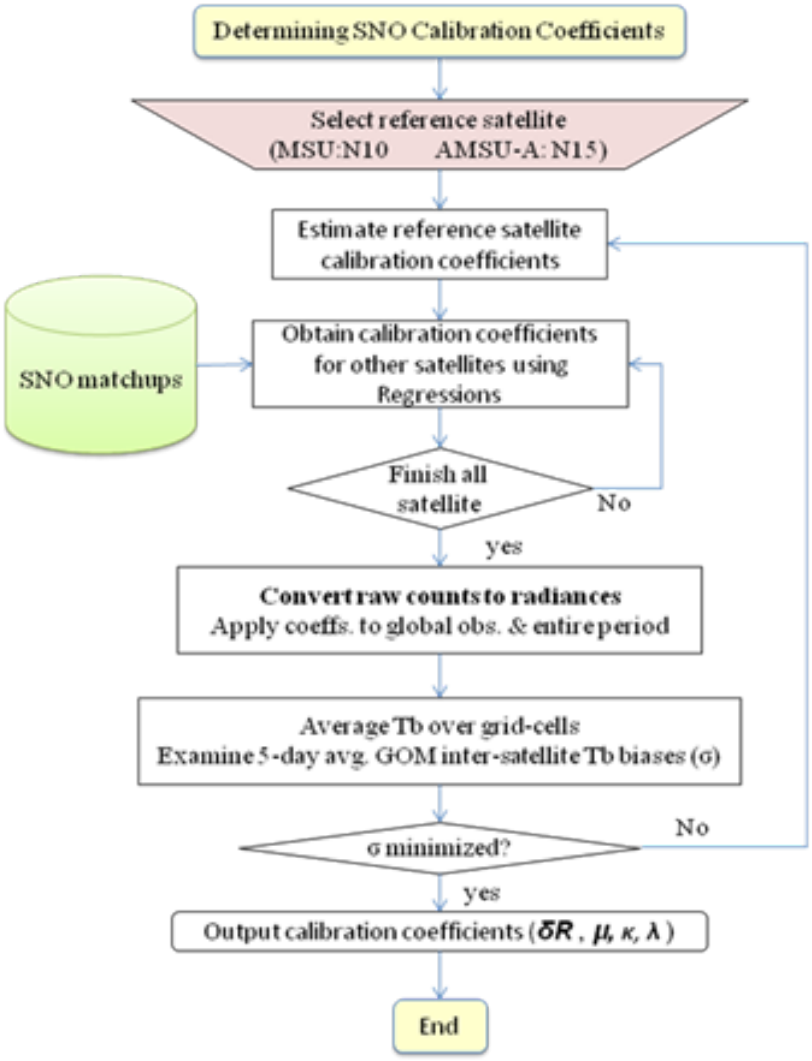

Figure 3-14 Sequential procedure for determining MSU/AMSU-A calibration coefficients.

3.4.2.1 The MSU Calibration Coefficients

By design, the sequential method minimizes inter-satellite biases, scene temperature dependency in biases, and the solar-heating induced instrument temperature variability in the radiances. In the MSU case, optimal calibration coefficients were obtained for all satellites (Zou et al., 2009). Table 3-2 lists these calibration coefficients. Figure 3-15 demonstrates the performance of these coefficients by showing global ocean-mean inter-satellite brightness temperature difference time series from prelaunch calibration (Figure 3-15a) compared to those obtained from the IMICA calibration coefficients in Table 3-2 (Figure 3-15b). As seen, inter-satellite biases and the solar-heating induced instrument variability as observed in Figure 3-15a for NOAA-10 through NOAA-14 are mostly removed in Figure 3-15b. In addition, scene temperature dependency in biases were also significantly reduced (Figure 3-12).

Table 3-2 Calibration coefficients for MSU channels 2, 3, and 4 for different satellites obtained from the SNO sequential procedure, where δR is the offset and μ the nonlinear coefficient. Units for δR and μ are 10-5 (mW) (sr m2 cm-1) -1 and (sr m2 cm-1) (mW)-1, respectively.

Satellite	Channel 2		Channel 3		Channel 4	
	δR	**μ**	***δR***	**μ**	***δR***	**μ**
NOAA TIROS-N	1.3963	5.4062	5.7535	1.2941	1.6808	4.8256
NOAA 6	0	7.3750	0.1162	6.1974	-1.5438	6.5032
NOAA 7	0	7.4380	-2.8131	10.4644	-1.9660	6.5637
NOAA 8	-1.3750	8.2636	1.4737	4.4531	-0.5083	5.5242
NOAA 9	-0.0771	5.9713	0.1026	9.0332	0.7721	6.1028
NOAA 10	0	6.2500	0	5.6300	0	4.9500
NOAA 11	-2.4641	9.5909	-1.9983	7.1892	-0.7271	5.4574
NOAA 12	-0.0996	6.7706	-2.3979	8.3282	-4.6074	7.1040
NOAA 14	-0.6363	7.4695	-3.0810	8.7524	-0.7753	5.4175

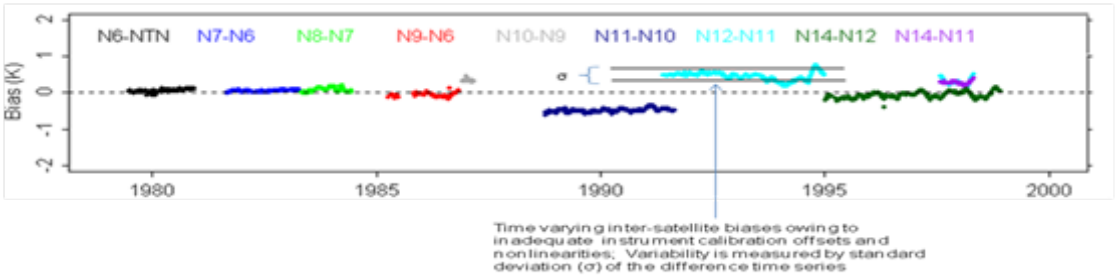

(a)

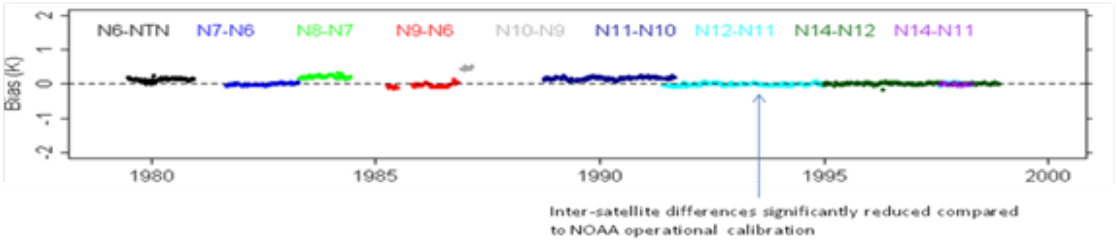

(b)

Figure 3-15 Global ocean-mean inter-satellite brightness temperature difference time series for MSU channel 2 onboard TIROS-N through NOAA-14 derived from (a) the NOAA operational calibrated radiances, and (b) radiances obtained from using SNO calibration coefficients.

3.4.2.2 The AMSU-A Calibration Coefficients

For AMSU-A observations, bias drifts and a combination of bias drifts and instrument temperature variability were observed in the pre-launch calibrated radiance time series for certain channels of NOAA-16 and MetOp-A. For these channels, constant offsets and nonlinear coefficients cannot remove their bias drifts. Therefore, time dependent offsets and nonlinear coefficients are introduced to account for the bias drifts (Zou and Wang, 2011). In specific, the following calibration offset model is assumed for MetOp-A channel 7 and most NOAA-16 channels,

$$\delta R = \delta R_0 + \kappa(t - t_0) \qquad (3\text{-}5)$$

where δR_0 is a constant offset, κ is a constant rate of changes in the offset, t is time, and t_0 is a reference time which can be the satellite launch time or other reference time when the offset begins to drift. Calibration results indicate that this offset model is sufficient to remove the bias drift in all channels except for NOAA-15 channel 6. For this channel, the nonlinear coefficient is also assumed to be time-dependent,

$$\mu = \mu_0 + \lambda(t - t_1) \qquad (3\text{-}6)$$

where μ_0 is a constant nonlinear coefficient, and λ is the rate of changes of the nonlinear coefficient, and t_1 is another reference time.

When solving for the calibration coefficients in Equations 3-5 and 3-6, δR_0 and μ_0 were obtained first from the SNO sequential procedure described earlier with λ and κ being assumed to be zero and NOAA-18 was used as the reference satellite. The resulting δR_0 and μ_0 were then fixed in Equations 3-5 and 3-6 in subsequent procedures where λ and κ values are determined. To obtain λ and κ, a series sensitivity experiments were conducted in which λ and κ were selected within a reasonable range and different set of level-1c radiances were computed corresponding to these different values. The final selection of λ and κ were made when the inter-satellite bias drifts of the global ocean means are minimal for all respective channels.

The resulting calibration coefficients for channels 4-14 onboard NOAA-15, -16, -17, -18 and MetOp-A are listed in Table 3-3. Aqua was recalibrated in the sense that only constant offsets were obtained since its raw counts are not easily acquired. Nevertheless, inter-satellite bias analysis as shown in Figure 3-12 indicated that no significant instrument temperature variability was found for all Aqua channels during the time period from its launch to present. Therefore, it is postulated that the non-linear calibration coefficients for Aqua AMSU-A may not need to be changed from those obtained in pre-launch calibration.

Table 3-3 SNO determined calibration coefficients for AMSU-A channels 4-14. For simplicity, all δR and μ were adjusted to the corresponding starting time shown in the equation (2001 for δR and 1998 for μ). These starting times were not necessarily set to be the exact launch time for a satellite. One can transfer them to the satellite launch time if needed by changing the values of δR_0 and μ_0. Calibration coefficients of AMSU-A surface channels 1-3 and 15 are not included. Units for δR_0, μ_0, κ, and λ are 10^{-5} (mW) (sr m^2 cm^{-1}) $^{-1}$, (sr m^2 cm^{-1}) $(mW)^{-1}$, (mW) (sr m^2 cm^{-1}) $^{-1}$ $(year)^{-1}$, and (sr m^2 cm^{-1}) $(mW)^{-1}(year)^{-1}$, respectively.

		δR_0	κ	μ_0	λ
Channel 4	NOAA-15	0	0	-0.269	0
	NOAA-16	0	0	-0.718	0
	NOAA-17	0.220	0	-0.886	0
	NOAA-18	0.276	0	0.929	0
	MetOp-A	0.324	0	0.442	0
	Aqua	-0.034	0	0	0
Channel 5	NOAA-15	0	0	0.3	0
	NOAA-16	-1.846	-7.248e-07	2.4	0
	NOAA-17	0.877	0	-1.007	0
	NOAA-18	0	0	1.468	0
	MetOp-A	0.467	0	0.262	0
	Aqua	0.023	0	0	0
Channel 6	NOAA-15	1.406	-0.614e-05	0	0.442
	NOAA-16	-2.903	-1.177e-06	4.3	0
	NOAA-17	5.065	0	-3.722	0
	NOAA-18	0	0	3	0
	MetOp-A	1.131	0	2.389	0
	Aqua	1.667	0	0	0
Channel 7	NOAA-15	0	0	0.3	0
	NOAA-16	-4.475	-1.570e-06	3.6	0
	NOAA-17	3.043	0	-2.347	0
	NOAA-18	1.319	0	0.479	0
	MetOp-A	2.152	-1.169e-06	0.396	0
	Aqua	-0.341	0	0	0
Channel 8	NOAA-15	0	0	0.667	0
	NOAA-16	-5.043	-1.768e-06	4.3	0

	NOAA-17	2.078	0	-1.099	0
	NOAA-18	0.440	0	0.964	0
	MetOp-A	1.633	0	0	0
	Aqua	-0.034	0	0	0
Channel 9	NOAA-15	0	0	0.077	0
	NOAA-16	-4.130	-3.936e-07	2.3	0
	NOAA-17	1.334	0	-0.809	0
	NOAA-18	-0.108	0	0.820	0
	MetOp-A	0.111	0	1.246	0
	Aqua	-1.403	0	0	0
Channel 10	NOAA-15	0	0	0.346	0
	NOAA-16	0.227	0	-0.200	0
	NOAA-17	0.711	0	-0.361	0
	NOAA-18	0.876	0	1.116	0
	MetOp-A	0.975	0	1.148	0
	Aqua	-0.189	0	0	0
Channel 11	NOAA-15	0.532	0	0.251	0
	NOAA-16	-0.788	2.910e-7	0.733	0
	NOAA-17	0.595	0	0.406	0
	NOAA-18	0	0	1.500	0
	MetOp-A	0.614	0	1.626	0
	Aqua	0	0	0	
Channel 12	NOAA-15	0	0	1.115	0
	NOAA-16	-0.300	-8.000e-7	1.600	0
	NOAA-17	1.752	0	0	0
	NOAA-18	3.390	0	0	0
	MetOp-A	3.662	0	0	0
	Aqua	1.754	0	0	0
Channel 13	NOAA-15	0	0	1.500	0
	NOAA-16	0.702	-8.045e-07	1.000	0
	NOAA-17	1.471	0	0	0
	NOAA-18	3.171	0	0	0
	MetOp-A	3.018	0	0	0
	Aqua	2.696	0	0	0

Channel 14	NOAA-15	0	0	0	0
	NOAA-16	-1.364	-0.154e-5	1.200	0
	NOAA-17	-0.514	0	0.712	0
	NOAA-18	0	0	0.600	0
	MetOp-A	-0.062	0	-0.435	0
	Aqua	0	0	0	0

The global ocean mean inter-satellite difference time series for channel 5, 6, 7, and 9 derived respectively from operational calibration and the calibration coefficients in Table 3-3, are shown in Figures 3-16 and 3-17. As seen, inter-satellite biases, solar heating induced instrument temperature variability, and bias drift are all found in Figure 3-16 in the operational calibration. These biases are all significantly reduced by the SNO calibration coefficients. The biases and standard deviation of the inter-satellite difference time series in Figure 3-17 are typically on the order of 0.05K and 0.03 K, respectively, compared to 0.5 K and 0.13 K in prelaunch calibration shown in Figure 3-16.

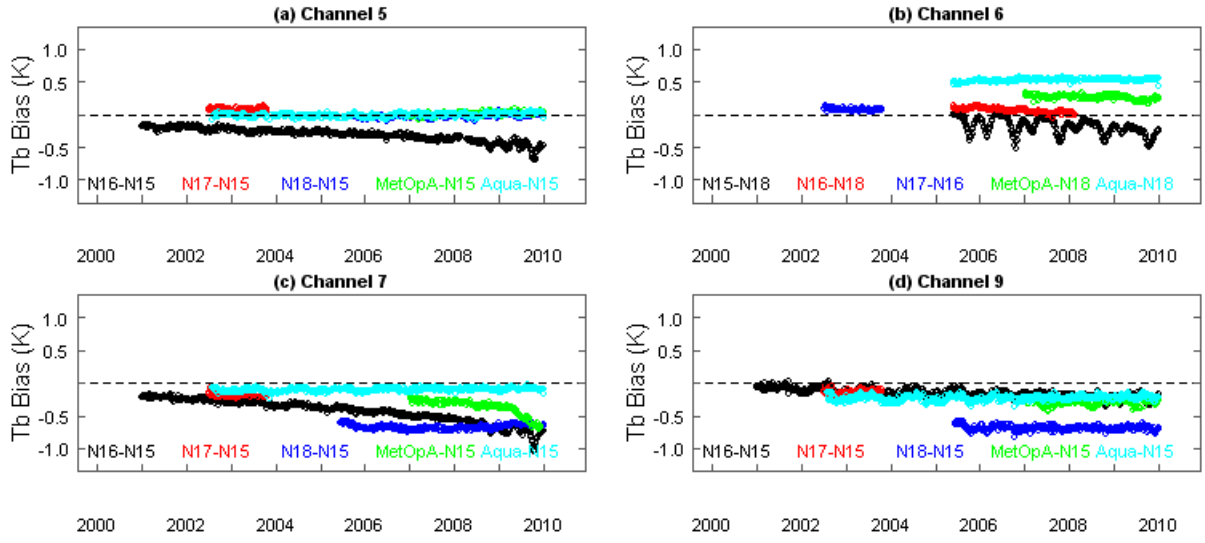

Figure 3-16 Global ocean-mean inter-satellite Tb difference time series for AMSU-A operational calibration for satellites NOAA-15, -16, -17, -18, MetOp-A, and Aqua for different channels. Differences are chosen against the reference satellites, thus the satellite pairs shown for channel 6 are different from other channels.

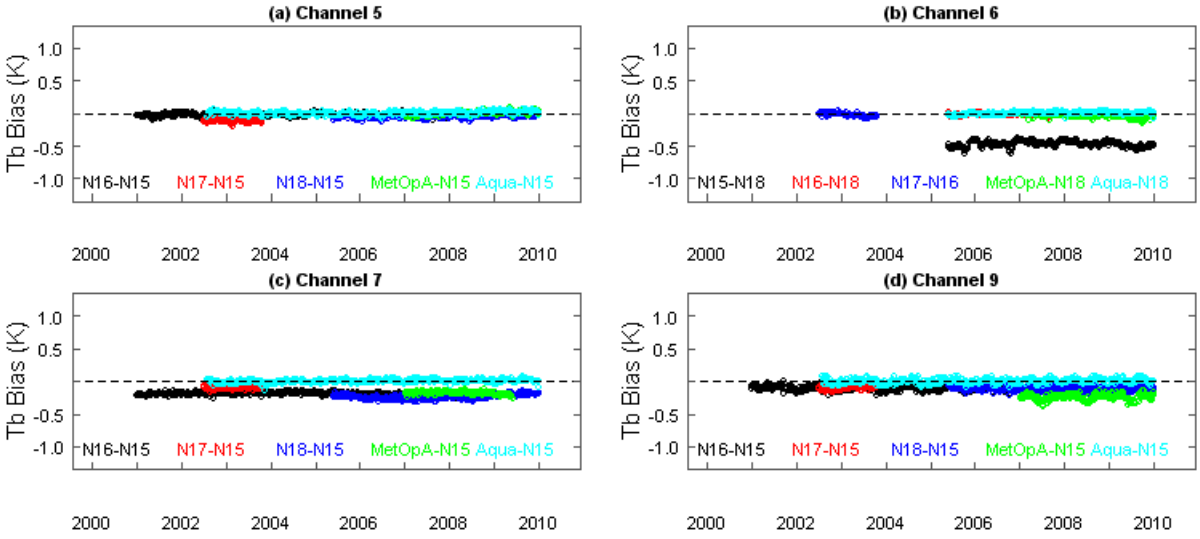

Figure 3-17 Same as Figure 3.16 except Tb is obtained using the SNO inter-calibration coefficients listed in Table 3-3. Note the large differences between NOAA-18 and NOAA-15 for channel 6 is caused by post-launch frequency shift in NOAA-15 channel 6. The correct frequency for NOAA-15 channel 6 has been obtained in Zou and Wang (2011), which is 36.25 MHz higher than pre-launch specification or measurements.

3.4.3 The Gridding Method for Generating AMSU-A Daily Gridded Brightness Temperature FCDR

The gridding algorithm mainly includes 4 parts:

i. Temporal alignment to remove repetitive data

ii. Splitting orbit

iii. Mapping swath data to grid

iv. Composing gridded FCDR with 3 strategies

3.4.3.1 Temporal Alignment

Temporal alignment is used to remove repetitive scans in level-1c files. For AMSU-A, thirty contiguous scene resolution cells are sampled in a stepped-scan fashion every eight seconds. As a result, there should be exactly 10800 scans in total for each day. Although time of the first scan may vary by satellite, there should be only one scan for every 8 seconds. Let t represent the time from mid-night (00:00:00) in seconds and divide the 24 hours of a day into 10800 temporal slots $\{T_k\}_{0\le k<10800}$ with 8 seconds interval, i.e.

$$T_k = \{t|\ (t \ge k * 8)\ \ and\ (t < (k+1) * 8)\ \}, 0 \le k < 10800, \qquad (3\text{-}7)$$

For each day, there should be only one AMSU-A scan for a satellite in each of the temporal slots. Temporal alignment is thus implemented as follows:

1) For each day, identify a list of available level-1c files for the period of 24 hours.

2) Create an array of flag with 10800 elements to record the status of each temporal slot, initialize the flags to 0.

3) For each level-1c file in the list, read data of each scan, and determine the slot of each scan according to scan time t_{scan}. The scan time in level-1c is seconds since 01/01/1978, so the slot for each scan can be calculated according to the following equation:

$$k = floor\left(\frac{t_{scan}-t_0}{8}\right), \quad (3\text{-}8)$$

where t_0 is time in seconds of the midnight (00:00:00) of a specific day since 01/01/1978.

Then a check of quality flag is conducted for each scan. If the scan is invalid, skip it. If the scan is valid, check the flag of the corresponding temporal slot. If the flag is 0, marks it as 1, and compose the scan data to daily records according to slot number. If the slot is already marked as 1, skip the current scan to avoid repetition. In cases no valid data are available for some slots due to bad scans, just fill the slot with invalid values. This allows alignment of the data in correct temporal order.

4) Finally, for each day, level-1c data with 10800 temporally-aligned scans are generated.

3.4.3.2 Splitting Orbit

The AMSU-A daily gridded brightness temperature FCDR data for ascending and descending nodes are generated separately. The AMSU-A level-1c radiance FCDR files do not have information on ascending and descending orbits; an algorithm to obtain such information is thus developed here. This is achieved by using the nadir geolocations to split ascending and descending orbits for the 10800 temporally-aligned scans for each day. Nadir geolocation is calculated approximately using the near nadir scan positions 15 and 16 with the following equations:

$$Lat_{nadir} = (Lat_{15} + Lat_{16}) * 0.5, \quad (3\text{-}9)$$

$$Lon_{nadir} = (Lon_{15} + Lon_{16}) * 0.5, \quad (3\text{-}10)$$

where (Lat_{15}, Lon_{15}) and (Lat_{16} , Lon_{16}) are the (latitudes, longitudes) of the scan positions 15 and 16, respectively.

Orbits are determined according to the following rule: for each scan, if its nadir latitude is larger than the nadir latitude of the previous scan, it belongs to ascending orbits; otherwise, it belongs to descending orbits.

3.4.3.3 Mapping Swatch Data to Grid

The grid of the FCDR has a 1°×1° resolution, with longitude from -179.5° to 179.5° and latitude from 89.5° to -89.5°. Consequently, the data grid has 180 rows from 0 to 179, and 360 columns from 0 to 359. For each pixel, its row and column on the 1°×1° grid are determined from the following equations:

$$row = floor(90 - latitude), \quad (3\text{-}11)$$

$$col = flor(longitude + 180), \quad (3\text{-}12)$$

Using equations (3-11) and (3-12), all pixels from scan positions 8 to 23 are mapped into the grid for further processing in composition. Data gaps exist since many grid cells may not have valid observations because of quality control and the limited spatial coverage for daily data.

3.4.3.4 Composing Daily Gridded Brightness Temperature FCDR

Three different composing strategies were used to generate daily gridded AMSU-A brightness temperature FCDR: 1) near-nadir only; 2) minimum view zenith angle (closest to the nadir); and 3) means from the scan positions 8-23 for limb-corrected brightness temperatures.

1. Daily near-nadir only FCDR product

For each cell of the 1°×1° grid and for each channel, the availability of valid near-nadir pixels for the scan positions 15 and 16 of the IMICA L1c FCDR products are checked. There are 3 situations: no valid near-nadir pixels can be found; only one valid near-nadir pixel is found; and more than one valid near-nadir pixels are found. In the first situation, the cell is filled with invalid value. In the second situation, the grid cell temperature is represented by the only valid pixel from the L1c FCDR. In the third situation, averages of the multiple near-nadir pixels are used to represent the grid cell temperatures.

2. Daily minimum-view-angle FCDR product

For each cell of the 1°×1° grid and for each channel, the availability of valid pixels for the scan positions 8-23 of the IMICA AMSU-A FCDR products is checked. There are also 3 situations: no valid pixels available; only one valid pixel available; and more than one valid pixels available. In situation 1, the cell temperature is represented by missing value. In situation 2, the only valid pixel from the AMSU-A L1c FCDR is selected to represent the grid cell temperature. Scan time and view zenith angle of the pixel are then saved as part of the gridded FCDR products. In situation 3, the pixel with the minimum view zenith angle is selected among the multiple pixels found in the grid cell to represent the grid cell brightness temperature. The scan time and view zenith angle of the selected pixel is then saved as part of the gridded FCDR products.

3. Daily mean FCDR product

For each cell of the 1°×1° grid and for each channel, the availability of valid pixels for scan positions 8-23 of the limb-corrected IMICA AMSU-A FCDR products is checked. There are also 3 situations: no valid pixel is available; only one valid pixel is available; and more than one valid pixels are available. In situation 1, the cell temperature is represented by missing value. In situation 2, the only valid pixel from the L1c FCDR is used to represent the brightness temperature of the grid cell. In situation 3, the mean and the standard deviation of all the valid pixels are calculated and saved to represent the brightness temperature and its statistical error for the grid cell.

3.4.4 Numerical Strategy

The computation of the IMICA recalibrated radiances is straightforward using Equation 3-3 given the calibration coefficients and the raw counts data from the Earth views, target views, and other necessary parameters from the MSU/AMSU level-1b files. Processing the large amount of AMSU level-1b files and saving the resulting level-1c files require tens of Terabytes of disk space storage. Frequent update of the disk storage and workstations for processing the dataset needs to be planned ahead.

The computation of gridded brightness temperature FCDR is also straightforward using the equation and composing strategies as described above. Processing the large amount of the AMSU-A level-1c FCDR files and writing the resulting gridded brightness temperature FCDR files require several terabytes of disk space storage.

3.4.5 Calculations

The algorithm steps for generating the radiances are as follows:

1) Read ancillary datasets including calibration coefficients
2) Processing each MSU/AMSU level 1b orbit file
   - Read level 1b header
   - Process each scan line
     - Parse scan line
     - Calibrate scan line using Equation 3-3 for each footprint
     - Run precipitation detection program to identify if the footprint observation is precipitation contaminated
     - Run quality control program to ensure the calibrated radiance is valid
   - Generate Level-1c radiance file
   - Output the Level-1c file using NetCDF format
3) Repeat step 2) for another L1b orbit file
4) Stop after all level 1b files are processed

The calculation steps for generating AMSU-A daily gridded brightness temperature FCDR are as follows:

1) Specify satellite and time period for generating the gridded brightness temperature FCDR.
2) For each day during a satellite operational period
   - Identify list of AMSU-A level-1c radiance FCDR files;
   - Run quality control and temporal alignment to get daily level-1c data with 10800 scans;
   - Split the daily level-1c data into ascending and descending nodes according to nadir geolocation approach;
   - Map daily level-1c data of ascending and descending nodes into the 1°×1° grids;
   - Composing daily gridded brightness temperatures according to the 3 different strategies;
   - Output the daily gridded brightness temperature data into files using NetCDF format.
3) Repeat step 2 for another day
4) Repeat step 1 for another satellite
5) Stop after all the daily gridded brightness temperature FCDR for the specified satellites and periods are generated

3.4.6 Algorithm Output

The MSU/AMSU-A swath radiances are the major outputs from the IMICA recalibration algorithm. Quality flags are produced to indicate product quality, invalid or missing data. The algorithm also outputs NOAA pre-launch calibrated and linear calibrated radiances.

Table 3-4 Parameters in the supplied output data.

Parameters	Explanation
IMICA recalibrated radiances	Recalibrated radiances for the atmospheric temperature channels MSU: channels 2-4 AMSU-A channels 4-14
NOAA pre-launched calibrated radiances	NOAA pre-launched calibrated radiances for all channels MSU: channels 1-4 AMSU-A channels 1-15
Limb-adjusted, IMICA recalibrated radiances	IMICA Recalibrated and limb-adjusted radiances for the atmospheric temperatures MSU: channels 2-4 AMSU-A channels 4-14
Limb-adjusted, NOAA operational	NOAA operational calibrated and limb-adjusted radiances

calibrated radiances	for all channels MSU: channels 1-4 AMSU-A channels 1-15
Quality control	Scan line and pixel/channel level quality control information based on Level 1b quality control, level 1c precipitation screening, and limb-adjustment algorithms

AMSU-A daily gridded brightness temperature data are the primary output from the gridding algorithm. The following table summarizes the main contents of output using the three pixel-composition strategies. Data for ascending and descending nodes are output separately.

Table 3-5 Summary of the output data of the gridding algorithm.

Product	**Content**
Daily gridded near-nadir only FCDR	Daily brightness temperatures of the AMSU-A channels 4-14 from only the two near-nadir scan positions 15 and 16
Daily gridded minimum_view_angle FCDR	Daily brightness temperatures and scan time of the AMSU-A channels 4-14 from scan positions with minimum view zenith angle in a grid cell
Daily gridded mean FCDR	Mean and standard deviation of the limb-adjusted brightness temperatures of the AMSU-A channels 4-14 from scan positions 8-23

4. Validating Datasets and Algorithm Accuracy

4.1 Validating Datasets

Determination of accuracy and precision of the IMICA inter-calibration algorithm and its resulting FCDR are segmented into two parts: relative error estimates between satellite pairs and absolute error estimates with respect to an absolute truth. The purpose of the IMICA method is to improve inter-satellite calibration; evaluation of the relative errors between satellite pairs is thus the primary goal in the algorithm validation. However, absolute error estimate should also be carried out whenever possible since improving absolute accuracy is the ultimate goal of any calibration process. Ideally, absolute error estimate should be made against a SI-traceable standard of the microwave observations. However, such a standard does not exist at the time of this writing; therefore, various vicarious validation data sources are examined to determine their validity for validating the absolute accuracy of the IMICA inter-calibration algorithm. Such vicarious data sets are also rare due to the strict criteria required for a dataset to be of climate quality for validating other data sets: high precision and accuracy traceable to SI standards, long-term availability and stability, and global coverage with homogeneity. Since accuracy estimates for a calibration algorithm actually depend on the accuracy of the vicarious datasets themselves, cautious views of the estimating results are recommended. After reviewing available long-term temperature datasets in the climate science community, it is concluded that only the multi-year (2001-present) temperature retrievals from the Global Positioning System (GPS) Radio Occultation (RO) and reanalysis datasets have the potentials to serve as vicarious datasets to validate the IMICA calibrated MSU/AMSU radiances. Estimates of the relative accuracy of the IMICA calibration algorithm are made against those from pre-launch calibrations. The characteristics of these datasets and their comparison results with the IMICA calibrated MSU/AMSU observations are described as follows.

4.1.1 Pre-launch calibrated MSU/AMSU radiances

Advantages of the IMICA calibration algorithm are established by comparing inter-satellite biases against those from the pre-launch calibration. Pre-launch calibration is conducted independently for each instrument where calibration offsets are assumed to be zero and nonlinear calibration coefficients are obtained from laboratory test datasets (e.g., Mo, 2006). Time-varying inter-satellite biases exist for these instrument observations after launch. These data are available in the operational MSU/AMSU L1b files and they have been widely used in NWP data assimilations to improve NWP weather forecasting. The inter-satellite biases of the pre-launch calibrated datasets are used as reference for the IMICA calibration to compare with and for understanding the improvement of the latter algorithm compared to the former algorithm.

4.1.2 GPSRO data

The GPSRO data are provided by receivers onboard low Earth orbiting (LEO) satellites. As an LEO satellite sets or rises behind the Earth's limb relative to the GPS

transmitter satellite, the onboard GPS receiver takes measurements of the phase and amplitude of the GPS signals. These phase measurements, together with the precise knowledge of the positions and velocities of the GPS and LEO satellites, can be collectively used to derive accurate information (< 0.5 Kelvin temperature accuracy between ~5-25 km) on the thermodynamic state of the atmosphere. GPS RO data are minimally affected by aerosols, clouds, or precipitation and are not expected to have instrument drift and satellite-to-satellite instrument bias. Current evidence shows that temperature profiles acquired with GPS RO are absolutely stable at a level of <0.05 Kelvin between ~10-25 km, where the water vapor effects are small. In the middle and lower troposphere, refractivity datasets can be used instead of temperature, thus combining the temperature and moisture information.

In contrast to the microwave sounders, the raw GPS RO measurement is not based on a physical device that deteriorates with time — their performance is directly traceable to an absolute SI standard: International Atomic Time. Consequently, there is no need for calibration. This makes this limb-sounding technique extremely useful for calibration of other nadir sensors. Even if the span period of available RO measurements is not long enough (2001-present) to build GPS RO time series for climate applications yet, it can still be used to validate other observations such as MSU/AMSU stratospheric channels.

4.1.3 Reanalysis datasets

Reanalysis data were generated from long-term runs of fixed climate modeling systems with combinations of a comprehensive set of physical parameterizations and assimilation of routine observations from various sources such as satellites, ships, buoys, aircraft, and the radiosonde network, etc. The data assimilation process allows reanalysis to have a climate state favorable to certain input data, depending on human knowledge of bias nature of various input data as well as an appropriate bias correction scheme for the input data. Current generation of reanalysis systems employs a satellite bias correction scheme in their data assimilation sub-system. Satellite bias correction is a process to correct errors in satellite observations, including MSU/AMSU radiance data, before they are assimilated into modeling reanalysis systems. This correction is implemented based on the assumption that satellite data are less accurate compared to in situ observations such as those from radiosondes and aircrafts, which are not subject to bias correction before being assimilated into reanalysis systems. As such, when there is a disagreement between the satellite and radiosonde and aircraft observations, reanalysis data assimilation tends to generate a climate reanalysis favorable to the radiosonde and aircraft observations. Since in situ observations have biases relative to the absolute truth and are also subject to in-homogeneity in both time and space, the reanalysis data in principle cannot be treated as vicarious datasets for evaluating the absolute accuracy of the recalibrated MSU/AMSU FCDRs. Reanalyses developed by different operational centers are also different due to differences in their production processes which include climate modeling differences as well as different choices in input datasets and data assimilation schemes. These differences also cause difficulties in selecting appropriate reanalysis data for validating other climate datasets. Therefore, using reanalysis data to investigate the climate change or validate other dataset still comes a long way to go.

Despite these deficiencies, however, satellite bias correction techniques and their analysis are a unique tool that can provide independent assessment of the recalibration accuracies of the IMICA calibration algorithm. In particular, the bias correction patterns for individual satellites can be used to examine how well instrument calibration was conducted when compared to a reference climate favorable to in situ observations. New generation of reanalyses cover the entire satellite observation period, allowing evaluation of algorithm performance for the entire satellite observation period. An example of analysis will be provided in the following sections to demonstrate this feature.

4.2 Test Output Analysis

4.2.1 Reproducibility

4.2.1.1 The IMICA Calibration Algorithm

Based on characteristics of the validating datasets, different statistical methods are developed to determine the accuracy of the IMICA calibration algorithm. These include

a) In comparisons with pre-launch calibration, four statistical parameters are used to characterize the accuracy of the IMICA calibration. The details are described in the next section.
b) For GPSRO datasets, matched pixel observations of the MSU/AMSU and GPSRO data are first collected. Bias statistics of these matchups can characterize the accuracy and precision of the IMICA recalibrated MSU/AMSU radiances against GPSRO observations.
c) For reanalysis datasets, bias correction of the IMICA calibrated radiance data is analyzed. These bias correction analyses provide a fundamental understanding on the performance of the IMICA calibration algorithm in terms of how inter-satellite biases are removed when compared to a common reference dataset.

4.2.1.2 The Gridding Algorithm

The gridding algorithm described in this C-ATBD does not involve in any adjustment of the level 1C FCDR data; only temporal and spatial averaging with quality control was conducted on the L1C FCDR. As a result, the testing only requires to ensure that the gridding steps did not alter the original accuracy of the IMICA AMSU-A L1C radiance FCDR. In validation of the original IMICA AMSU-A level 1c FCDR, time series of global ocean mean and spatial patterns of inter-satellite biases were extensively used for accuracy assessment and analysis (Zou and Wang 2011). For the daily gridded FCDR developed here, similar checks were performed and compared with the validation results on the original level 1c FCDR data to validate the gridding algorithm. In particular, two inter-satellite bias patterns are generated to evaluate the accuracy and data quality of the gridded AMSU-A FCDR: a) Time series of inter-satellite global ocean mean differences which include both ascending and descending orbits; and b) Spatial patterns of inter-

satellite biases. The ocean mean difference time series can characterize the calibration biases very well since, for many AMSU-A channels, diurnal drift over the oceans are ignorable.

4.2.2 Precision and Accuracy

4.2.2.1 Relative Accuracy of the IMICA Inter-Calibration

Four parameters/indexes have been developed to evaluate the relative accuracy of the IMICA calibration algorithm between satellite pairs. These different parameters/indexes characterize different aspects in the instrument calibration errors. Advantages of the IMICA calibration algorithm are established by comparing values of these parameters against those from the pre-launch calibration.

i) Mean inter-satellite biases between SNO matchups—provide an estimate of the relative offsets between two satellites. The relative offsets arise from many different sources of calibration errors between satellite pairs: different offsets of the blackbody calibration targets, slight differences in antenna pattern corrections, differences in satellite height, etc. In pre-launch calibrated radiances, these biases are generally non-zero and are on the order of 0.3 to 1 K. An example has been shown in Figure 3-12a for the SNO matchups of MSU channel 2 between NOAA-10 and NOAA-11, where pre-launch calibrated radiances for the nadir pixels have a mean bias of 0.3 K. By definition, the SNO regression algorithm completely removes this bias, at least for the near nadir observations. As shown in Figure 3-12b, this bias is reduced to zero after the IMICA calibration.
ii) Scene temperature dependency in the inter-satellite biases — provide an estimate of the non-uniformity in inter-satellite biases. This type of biases occurs when calibration nonlinearity is inaccurate or when channel frequencies of two instruments are different. Bias structure in the scatter plot must be analyzed in order to determine the exact root-causes of the biases. In general, scene temperature dependent biases due to inaccurate calibration nonlinearity are characterized by a simple linear slope in the SNO scatter plot between two satellites (Figure 3-12), while those related to channel frequency differences have more complicated structures in the inter-satellite bias scatter plots. Fortunately, the first type of biases occurs more often than the second one. In addition, scene temperature dependency in biases causes the biases to depend on the latitude and season. The seasonal cycles in the SNO time series are thus defined as an associated parameter in characterizing the calibration accuracy in reducing scene temperature dependency in biases. The IMICA inter-calibration algorithm finds optimum nonlinear calibration coefficients which significantly reduce scene temperature dependent biases (Figure 3-12). As seen in Figures 3-12a and 3-12b, the SNO inter-calibration reduced the slope in the scatter plot by 3 times. Figure 4-1 shows another example of this type of biases between MetOp-A and NOAA-18 where seasonal cycles in the SNO time series are associated with slope in the SNO scatter plot between the two satellites. After SNO inter-calibration, the slope and the seasonal cycles in the SNO time series are both significantly reduced.

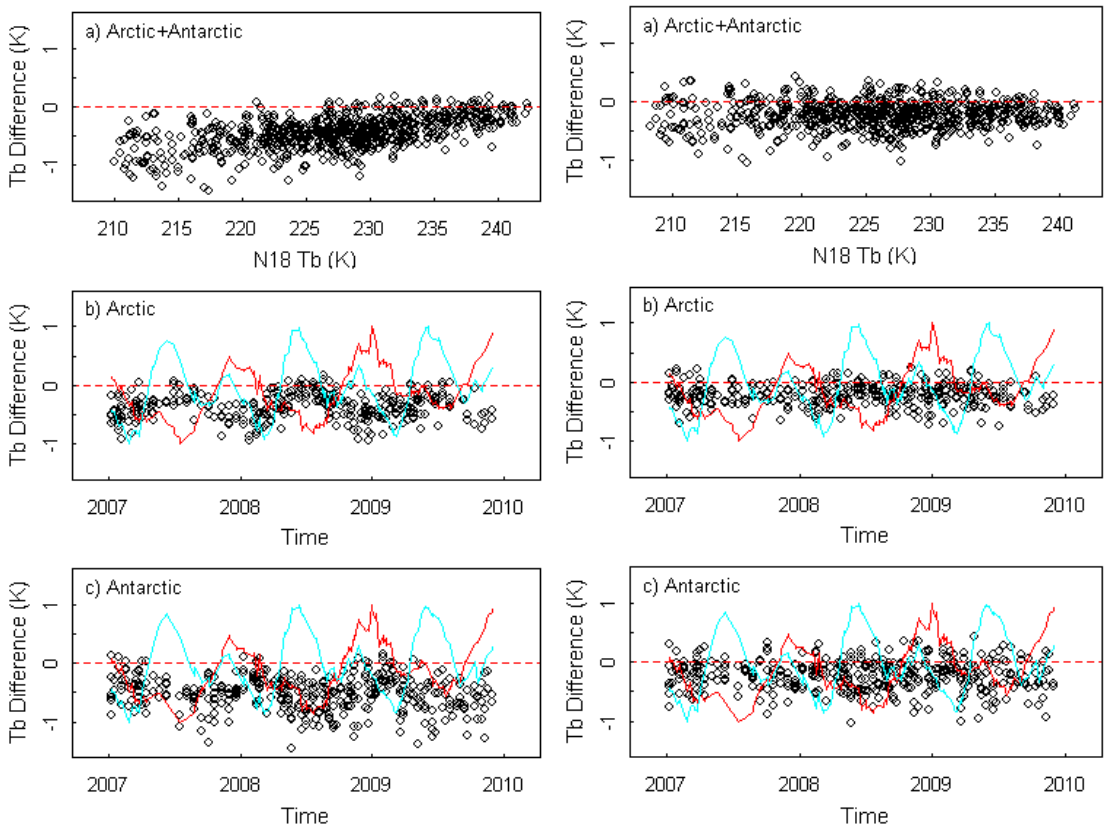

Figure 4-1 LEFT: a) SNO scatter plot for $T_b(N18)$ versus $\Delta T_b = T_b(MetOp-A) - T_b(N18)$; b) SNO time series for T_b (MetOp-A) - T_b (N18) over the Arctic; c) Same as b) except over the Antarctic. The T_b data in these plots were derived from unrealistic non-linear calibration coefficients assigned to both NOAA-18 and MetOp-A. The red and blue curves in b) and c) are the warm target temperature time series for MetOp-A and NOAA-18, respectively. The out-of-phase seasonality in the Arctic and Antarctic SNO time series cannot be explained by the warm target temperatures of either MetOp-A or NOAA-18. RIGHT: Same as LEFT except they are derived from SNO calibration coefficients.

Scene temperature dependent biases caused by channel frequency shift and their associated seasonal cycles in the Arctic and Antarctic SNO time series have been shown in Figure 4-2 for pre-launch calibrated observations of channel 6 between NOAA-15 and NOAA-18. After adjustment using the actual channel frequency value obtained from CRTM simulations, the scene temperature dependent biases in the SNO scatter plots between NOAA-15 and NOAA-18 and their SNO seasonal cycles are both removed (Figure 4-3).

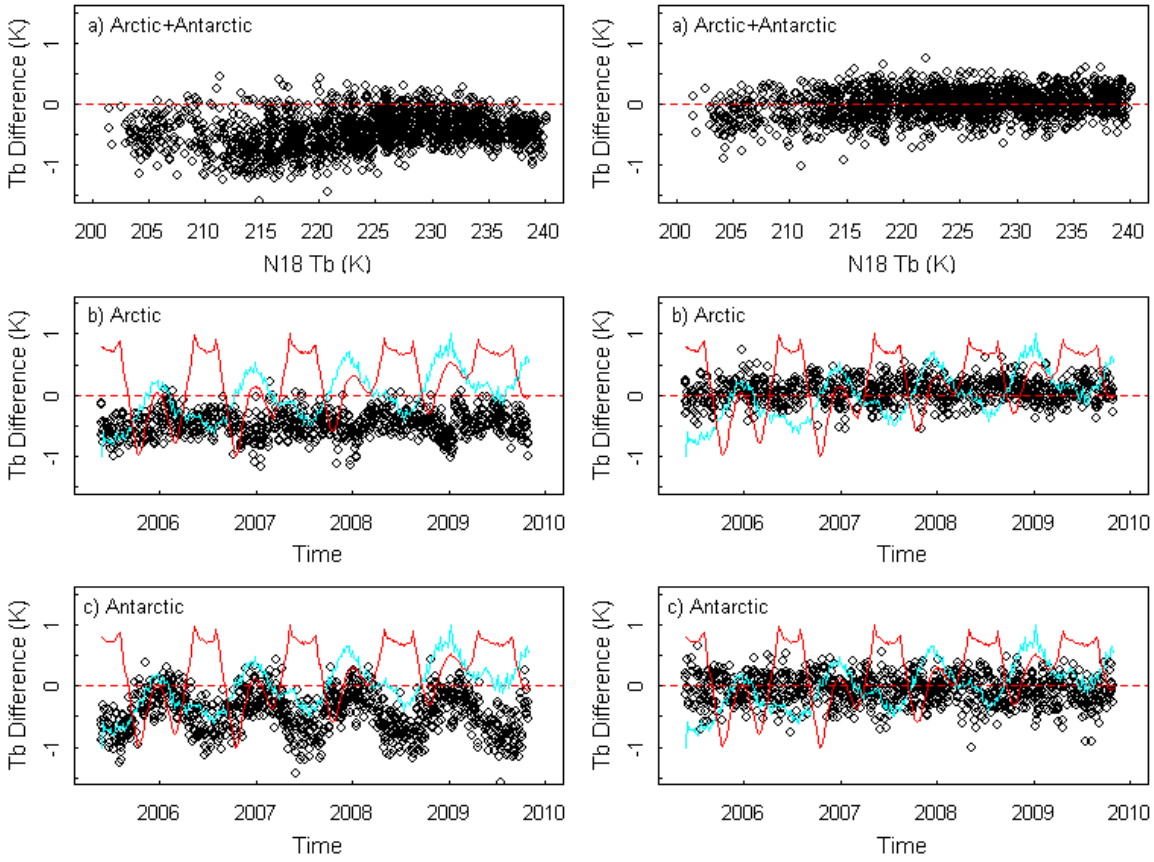

Figure 4-2 (LEFT Panels) a) SNO scatter plot for $T_b(N18)$ versus $\Delta T_b = T_b(N15) - T_b(N18)$; b) SNO time series over the Arctic for $\Delta T_b = T_b(N15) - T_b(N18)$; c) Same as b) except over the Antarctic. The T_b data in these plots were derived using the calibration coefficients in Table 3-3 where calibration non-linearity related scene temperature-dependent biases have already been minimized in the SNO calibration procedure. In addition, NOAA-15 offset has been adjusted to account for its frequency shift, so its T_b values are lower than operational calibrated values by a constant. The red and blue curves in b) and c) represent respectively the warm target temperatures of NOAA-15 and NOAA-18.

Figure 4-3 (RIGHT Panels) Same as Figure 4-2 except for the adjusted SNO time series between NOAA-15 and NOAA-18 in which the CRTM simulated differences due to the NOAA-15 frequency shift was subtracted from the observed NOAA-15 Tb.

iii) Latitudinal dependency in biases: Since the temperature range of the SNO matchups is slightly smaller than the global temperature range, removing biases and the seasonal cycles in the SNO matchups does not guarantee that biases are removed over the globe. It is desirable to examine scene-temperature-dependent biases in global datasets after the IMICA calibration. Latitudinal dependency in inter-satellite biases provides additional information on the calibration accuracies. Figure 4-4 shows the spatial pattern of the time-averaged T_b differences for NOAA-11 minus NOAA-10, NOAA-12 minus NOAA-11, and NOAA-14 minus NOAA-12 during their overlapping observations.

These figures include MSU channel 2 (T_2), channel 3 (T_3), and channel 4 (T_4) products. The figure shows that the biases are within ±0.1 K over the ocean and most of the land areas for the NOAA-14 minus NOAA-12 fields of T_3 and T_4 (Figure 4-4f). Similar bias level is also found for the differences between NOAA-12 and NOAA-11 and NOAA-14 minus NOAA-12 of T_2 over the oceans (Figure 4-4b,c). This shows the IMICA calibration works well over the globe for these overlaps. The NOAA-11 minus NOAA-10 of T_3 (Figure 4-4d) and the NOAA-12 minus NOAA-11 of T_4 (Figure 4-4h) show medium biases (±0.2 K) over the tropics. However, relatively larger differences (about 0.3 K) near the peaks of the Andes and Himalaya mountains are found for all overlaps for T_3 (Figure 4-4d–f). These larger differences occur because the surface elevation at these geographic locations is so high that the diurnal drift effect has a larger contribution to the channel 3 observations. For land areas with lower elevations, the diurnal drift effect is negligible for channels 3 and 4 as the inter-satellite biases over these areas are the same as over the oceans. In any situation, however, the diurnal drift effect for channel 2 is important over land because bias differences between land and oceans are more apparent (±1K over land but 0.2 K over oceans, Figure 4-4a–c). The NOAA-11 minus NOAA-10 of T_2 and T_4 (Figure 4-4a,g) and the NOAA-12 minus NOAA-11 for T_3 (Figure 4-4e) show larger latitudinal dependency, with smaller magnitude over the polar region and larger values over the tropics. This latitudinal dependency in biases suggests that a single calibration coefficient for the nonlinear term cannot completely remove the scene temperature dependency in biases. It is very likely that more terms and coefficients in the calibration equation are required for more accurate calibration when the quadratic approximation does not perform well.

iv) Inter-satellite biases of the global ocean mean time series—Although many calibration features can be characterized by the SNO matchups, global-ocean mean difference time series provide additional information on the bias characteristics of the calibrated radiances. This is because (a) global-ocean mean data include global temperature range which is larger than those from the SNO matchups which occur only over the polar region; (b) For many channels, global-ocean means do not have significant diurnal drift errors so they can still be used to characterize the instrument calibration errors; and (c) sample noise due to time and space differences in the SNO matchups is mostly cancelled out in the averaging process so the global ocean difference time series can be used to characterize some fine features such as the instrument temperature variability and long-term drift in the satellite radiance observations. By comparing the MSU global-ocean mean difference time series between satellite pairs before (Figure 3-15a) and after (Figure 3-15b) the IMICA calibration, the advantage of the IMICA calibration algorithm are seen from the following bias statistics: a) the inter-satellite biases in Figure 3-15b are about 0.1 K for the well-calibrated satellites such as NOAA-10 through NOAA-14, comparing to 0.5 K - 1 K in the pre-launch calibrated time series (for channel 3, inter-satellite biases as large as 2 K were observed in the pre-launch calibrated time series); b) warm target temperature variability are mostly removed in the IMICA calibration, resulting in the standard deviation of the global-ocean mean difference time series of only 0.03 K, compared to 0.12 K in the pre-launch calibrated time series (Figure 3-15a); c) there is no obvious bias drift in the IMICA calibrated difference time

series for all satellite pairs, while the bias drift in the pre-launch calibration is quite obvious, for example, between NOAA-12 and NOAA-14.

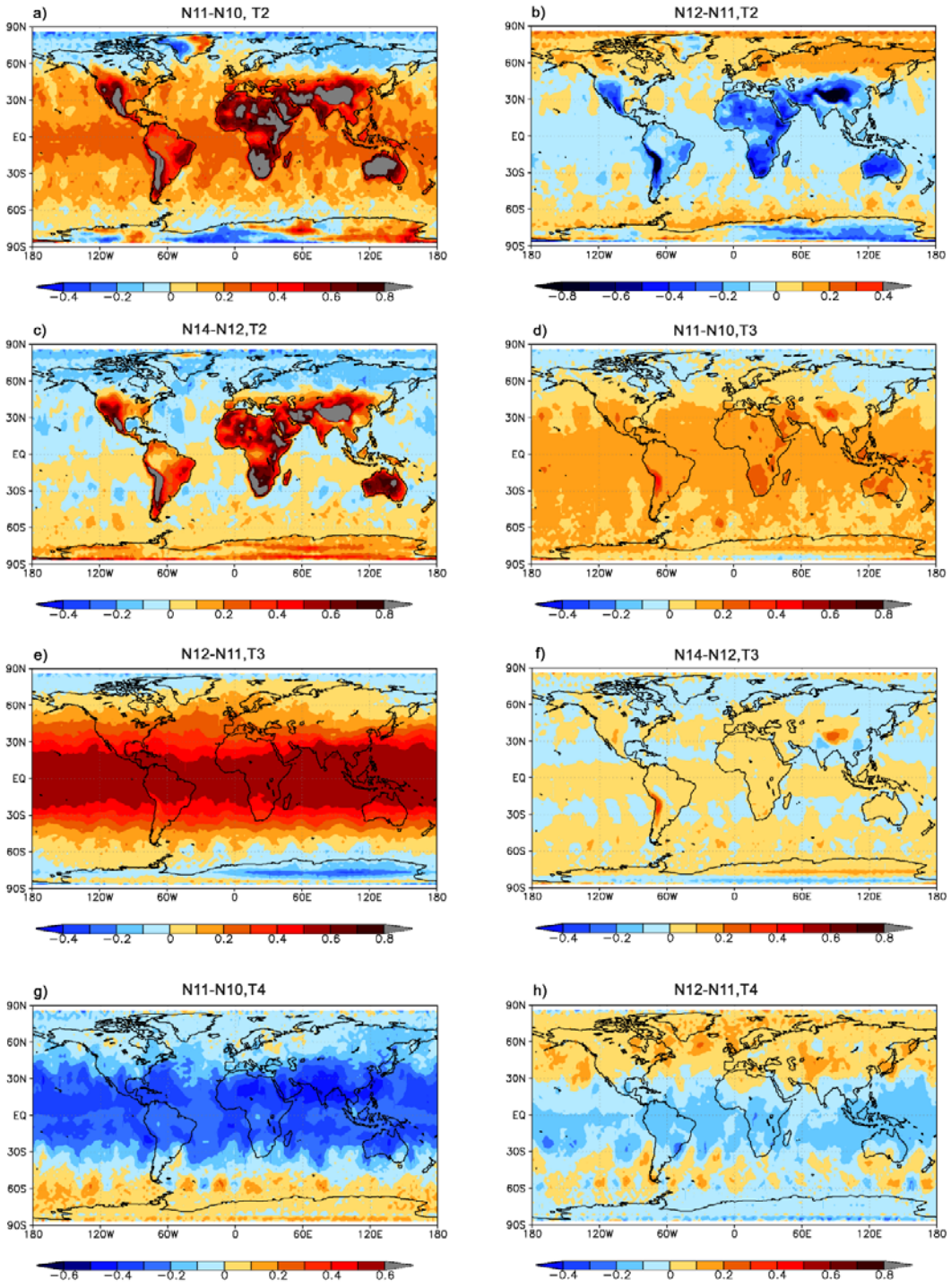

Figure 4-4 Intersatellite bias patterns for different satellite overlaps for different channels after the SNO calibration. A total of 7 limb-corrected footprints per scanline are used in

the pentad dataset. Units are in K.

4.2.2.2 Comparisons against GPSRO for Absolute Accuracy Estimates

Figures 4-5 and 4-6 compares the COSMIC retrievals with the AMSU-A channel 9 Tb derived from the IMICA calibration and the operational calibration for a randomly selected time period, July 2007. The comparisons are divided into three regions: Arctic (60°N-90°N, red dots), Antarctic (60°S-90°S, blue dots), and the rest of the Earth (60°N-60°S, green dots). Near nadir (the 15th footprint) and near limb (the 30th footprints) comparisons are provided separately. Table 4-1 further summarizes the bias statistics in the comparison.

The mean biases of the IMICA calibrated radiances are only of 0.01 K to 0.04 K for both the near nadir and near limb footprints, compared to a bias of about 0.30 K in the pre-launch operational calibrated data. This shows an obvious improvement from the IMICA calibration. Regional biases such as those over the Antarctic are much larger for both the IMICA and operational calibrations (0.3 K for IMICA and 0.8 K for the operational calibration) than those in the 60°N-60°S region. This suggests that either the COSMIC has a larger retrieval error (the GPSRO temperature was retrieved from the bending angle) or the AMSU-A data are downgraded over the polar region in both the IMICA and pre-launch calibrations. The IMICA uses two single parameters (nonlinear coefficient and offset) and two targets to calibrate the raw counts data. It is not likely that this calibration is downgraded over the polar region. Therefore, the problem is most likely related to deficiencies in the COSMIC retrievals. For instance, the polar stratospheric clouds may affect the accuracy of the COSMIC retrievals. This problem is being investigated at the time of this writing. This indicates that the comparison is not only useful in estimating the absolute accuracy of the IMICA calibrated radiances, but in turn, it is also helpful in identifying the potential problems in the validation dataset itself.

In addition, the slope of the IMICA calibration is closer to 1 in both the near nadir and near limb comparisons, suggesting less scene temperature dependency in biases in the IMICA calibrated radiances. These statistics indicate that the IMICA calibrated data are of higher accuracy and quality compared to the prelaunch calibration.

Table 4-1 Bias statistics in comparisons between COSMIC retrievals and the NOAA-15 AMSU-A channel 9 T_b for July 2007. The comparisons include operational (OPE) and the IMICA calibrated radiances (Table courtesy of Dr. Wenying He at Institute of Atmospheric Physics, China).

200707 N=957	60°S-60°N	60°N-90°N	60°S-90°S	Global
OPE-COSMIC	-0.25	-0.06	-0.82	−0.30
SNO-COSMIC	-0.01	0.07	-0.31	−0.04

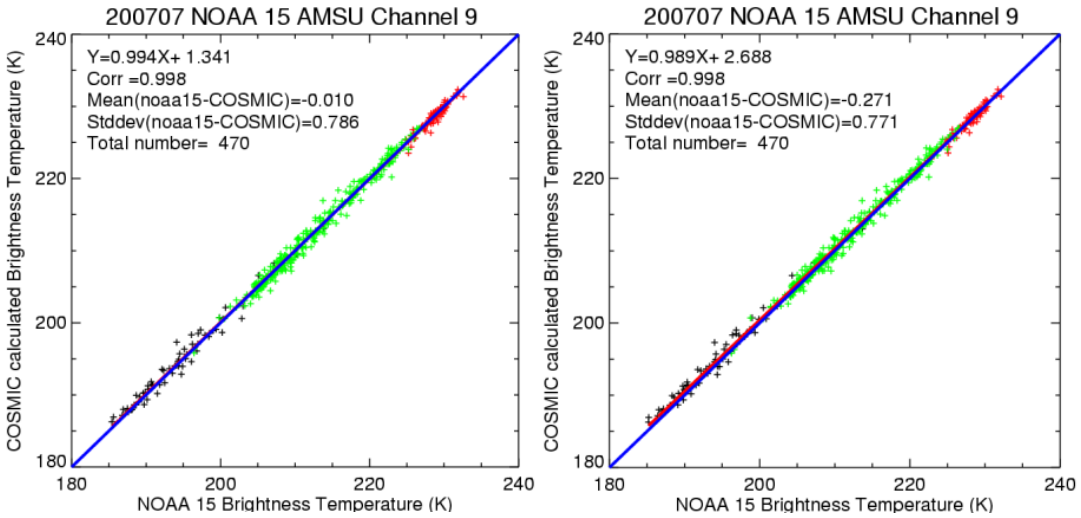

(a) (b)

Figure 4-5 Scatter plot between the AMSU-A channel 9 brightness temperature at the 15th footprint onboard NOAA-15 and the collocated COSMIC retrievals during July 2007. The red dots represent the Arctic (60°N-90°N) data, the blue dots the Antarctic (60°S-90°S) data, and the green dots for the rest of the Earth (60°N-60°S). (a) SNO calibrated radiances versus COSMIC; (b) Operational calibrated radiances versus COSMIC (Plots courtesy of Dr. Wenying He, Institutes of Atmospheric physics, China)

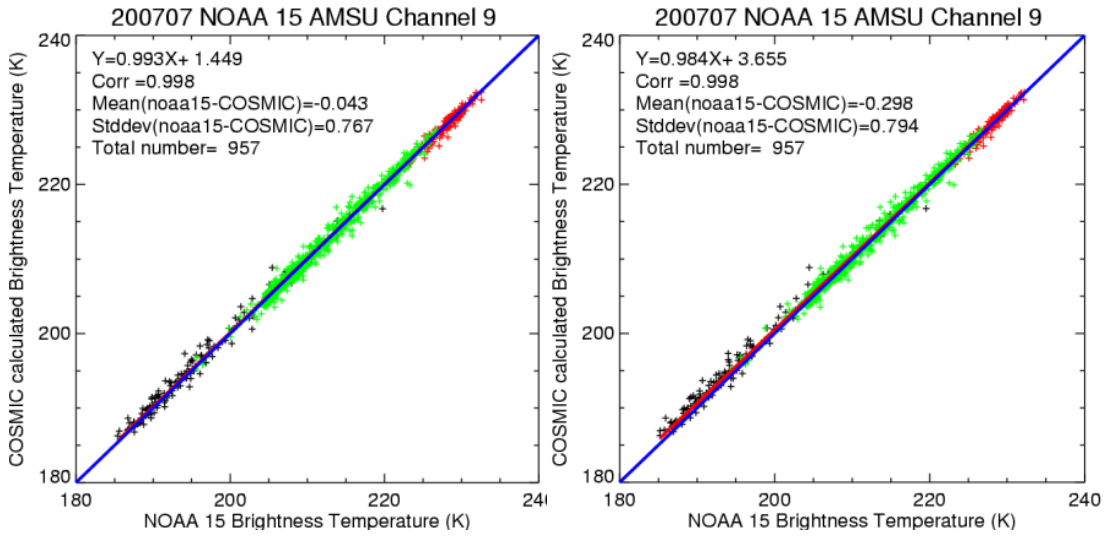

(a) (b)

Figure 4-6 Same as Figure 4-5 except for the 30th footprint.

4.2.2.3 Bias Corrections in Climate Reanalyses

The IMICA calibrated FCDR is expected to have good impact on the reanalysis bias correction process since the instrument calibration errors have been minimized. As an effort to test the performance of the inter-satellite calibration for climate reanalysis improvement, 20-years (1987-2006) of IMICA calibrated MSU level-1c radiances for channels 2, 3 and 4 onboard NOAA-10 through NOAA-14 were assimilated into the new generation of NCEP Climate Forecast System Reanalysis (CFSR) (Saha et al., 2010) and NASA Modern Era Retrospective-analysis for Research and Applications (MERRA) reanalysis (Rienecker, et. al. 2011). Since the CFSR and MERRA reanalysis cover the entire period of MSU observations from 1978 to 2006, they actually assimilated two different MSU level-1c data: the NOAA operational calibrated for TIROS-N through NOAA-9 and the post-launch IMICA calibrated for NOAA-10 through NOAA-14. The fact that radiances from these different calibrations were assimilated into a same system serves as an ideal experiment for evaluating the impact and performance of the IMICA inter-satellite calibration. Figure 4-7 shows the total bias correction patterns of MSU channel 2 in CFSR for the eight satellites from NOAA-6 through NOAA-14. The total bias correction is a global mean difference between the satellite observations being assimilated into the reanalysis and a background forecast field used to evaluate the observational biases. In many situations, the total bias correction is nearly the same as the difference between the observations and the final reanalysis field (O-M). Therefore, the total bias correction is an indicator of how well climate reanalysis agrees with the observations. The total bias correction for different satellites also measures the difference or agreement between different satellites, since double differencing of the bias corrections between two satellites leads to the same results as the inter-satellite bias analysis shown in Figure 3-15.

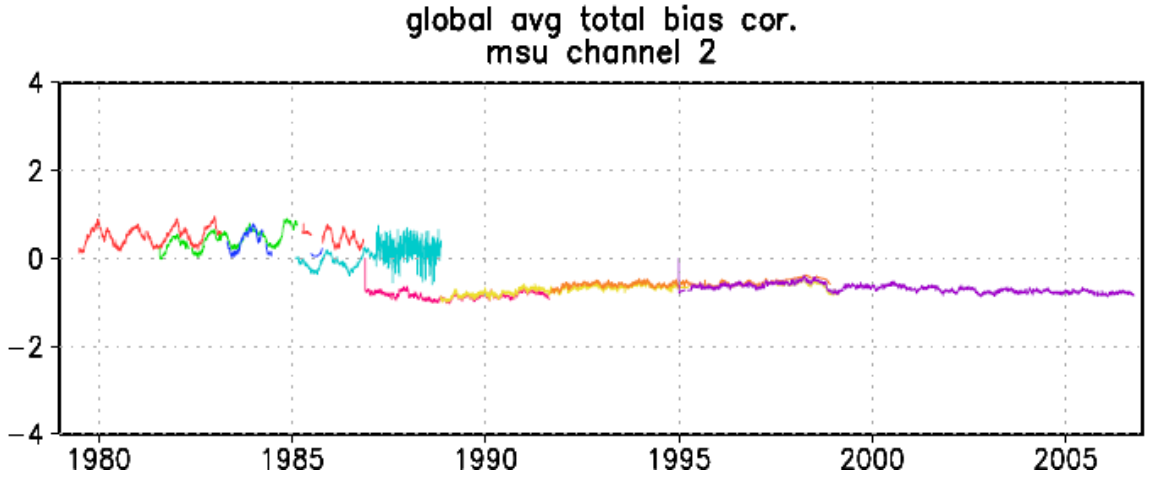

Figure 4-7 Four times daily averaged, global-mean total bias correction (Kevin) for MSU channel 2 onboard satellites from NOAA-6 through NOAA-14. The time series from 1979 to 1988 in 4 different colors (with larger seasonal variability) are for NOAA-6 through NOAA-9, and the smoother time series from 1987 to 2007 in other 4 different colors are

for NOAA-10 through NOAA-14 (Plot from (Saha et al., 2010)).

In Figure 4-7, the bias corrections for NOAA-6 through NOAA-9 exhibit obvious seasonal and inter-annual variability. This variability is related to the solar heating induced instrument temperature variations. In addition, the bias correction values for NOAA-6 through NOAA-9 are different for different satellites, indicating larger relative offsets between these satellites. This occurs because each individual satellite was calibrated independently in pre-launch calibration. In contrast, no instrument temperature variability is observed in bias corrections of the IMICA calibrated MSU observations for NOAA-10 through NOAA-14. Moreover, the bias correction values for NOAA-10 through NOAA-14 are nearly the same, resulting in much consistent bias correction patterns for these satellites. With a double differencing of the bias corrections for the IMICA calibrated satellites, one can see that the bias corrections are consistent with Figure 3-15 where inter-satellite biases are quite small for NOAA-10 through NOAA-14. In summary, bias correction pattern analyses indicate that the inter-calibrated MSU data have reached their performance expectation in reanalysis data assimilation.

One remaining problem is that there exist relative biases between the reanalysis climate and recalibrated satellite observations. Part of these errors may come from the climate reanalysis since it is not the truth. The other reason is that the absolute value of the inter-calibrated MSU/AMSU brightness temperature has not been adjusted to an absolute truth, although inter-satellite biases have been removed. As described earlier, the calibration offset of the reference satellite was arbitrarily assumed to be zero. This assumption does not affect the variability and trend analysis of the subsequent products developed from the FCDR. However, it influences the relative biases between the reanalysis and FCDR. This offset needs to be determined in FCDR validation processes against certain reference observations, ideally SI-traceable standards. Plans for such a validation are being developed at NOAA/NESDIS as part of the effort of MSU/AMSU FCDR development.

4.2.2.4 Temporal and Spatial Analysis of AMSU-A Daily Gridded FCDR

Time series of inter-satellite differences provide temporal characteristics on satellite accuracy. Figures 4-8 to 4-10 show the time series of daily brightness temperature inter-satellite differences for channels 5 over the global ocean for the three different types of gridded FCDRs. The time period for the time series is from beginning of 2001 to the end of 2014. The overall temporal patterns of the difference time series are consistent with those of the original IMICA AMSU-A level-1c data as analyzed in Zou and Wang (2011). This indicates that the gridding algorithms are correct.

Figures 4-11 to 4-13 show the spatial patterns of mean inter-satellite differences for channel 5 over the period from 01/01/2006 to 12/31/2014. The overall spatial patterns are consistent with those of the original IMICA AMSU-A level-1c data as analyzed in Zou and Wang (2011). This again indicates that the gridding algorithms are correct.

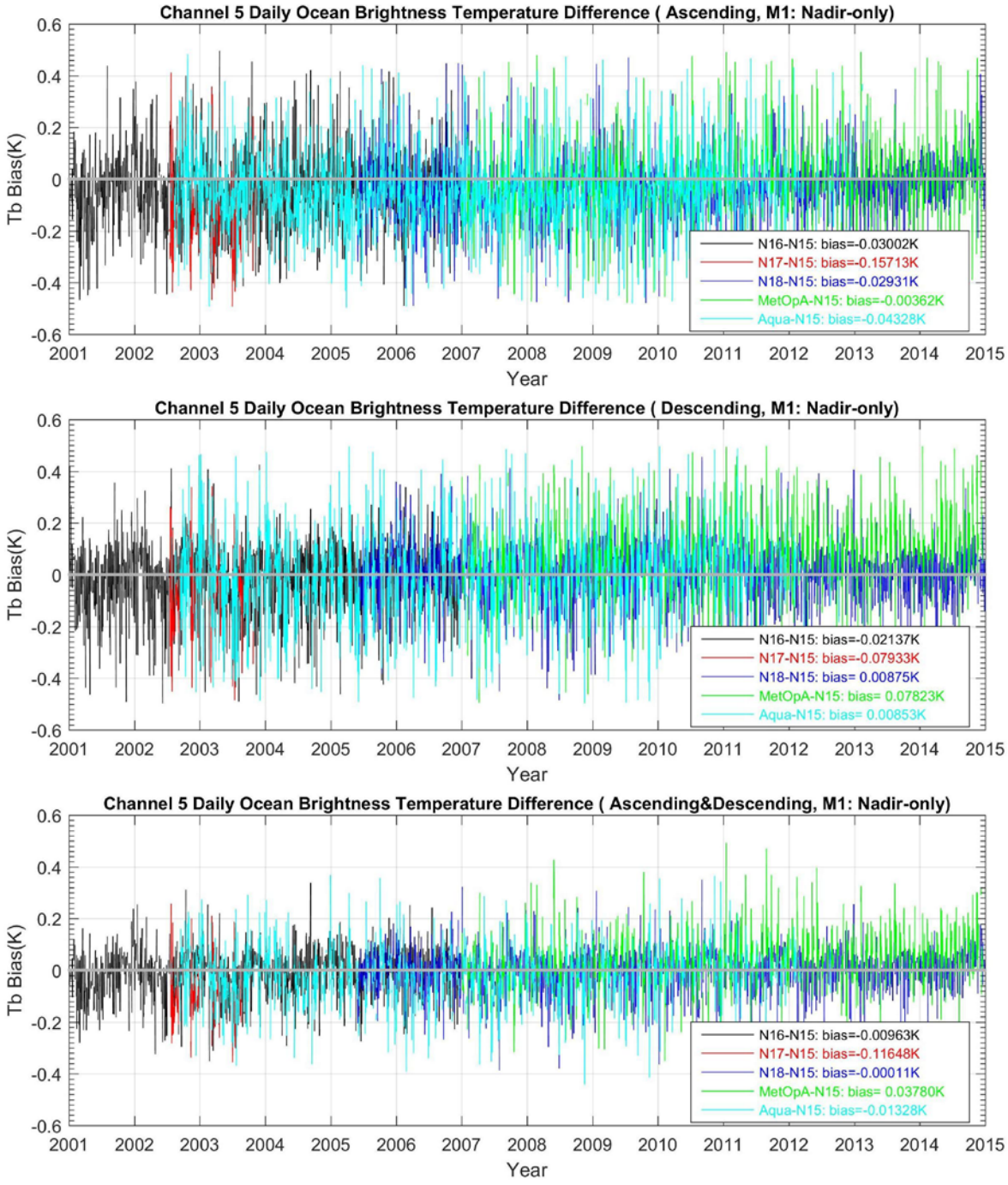

Figure 4-8 Time series of channel 5 daily ocean brightness temperature difference between satellite pairs of the nadir-only gridded FCDR.

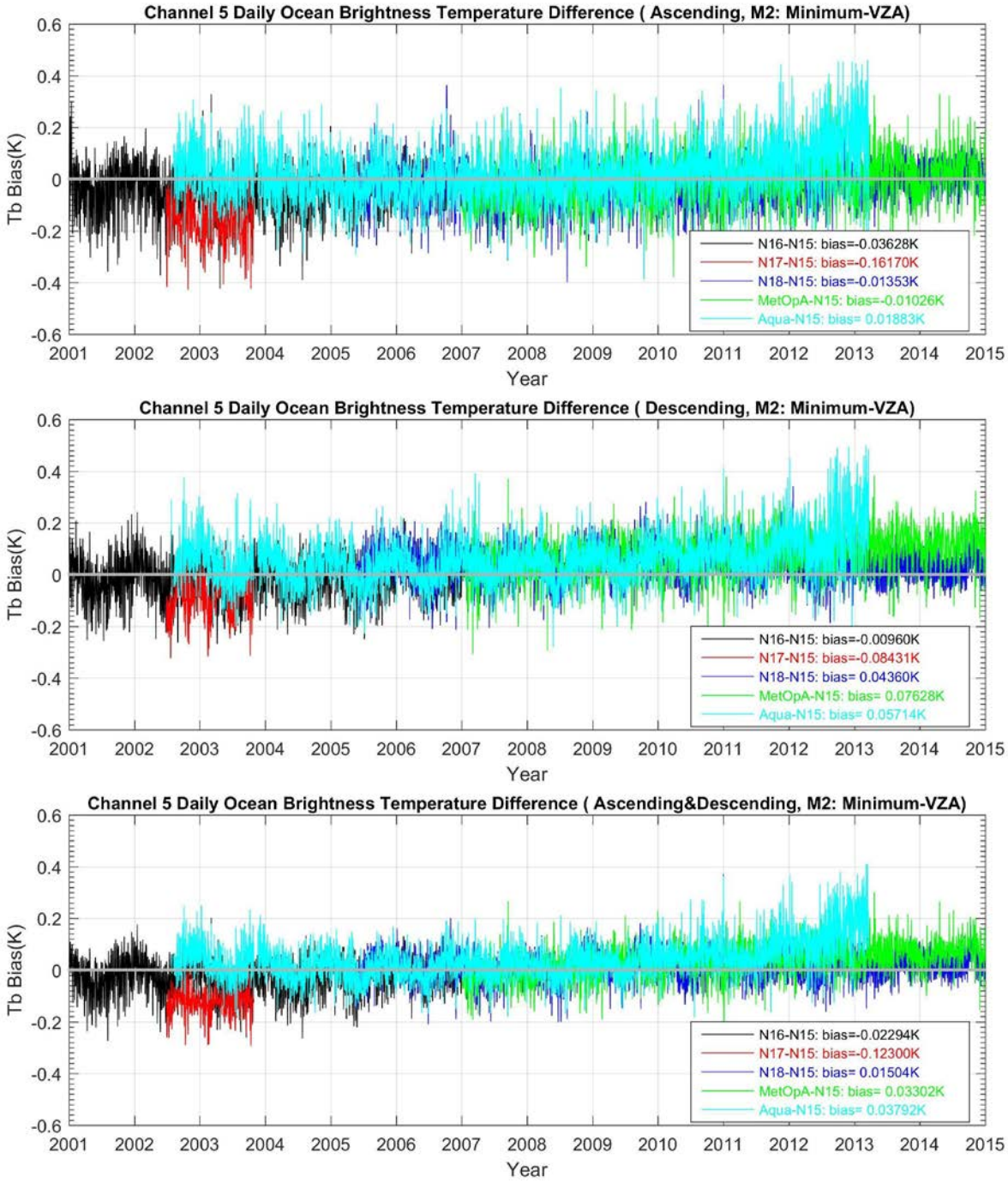

Figure 4-9 Time series of channel 5 daily ocean brightness temperature difference between satellite pairs of the minimum-VZA gridded FCDR.

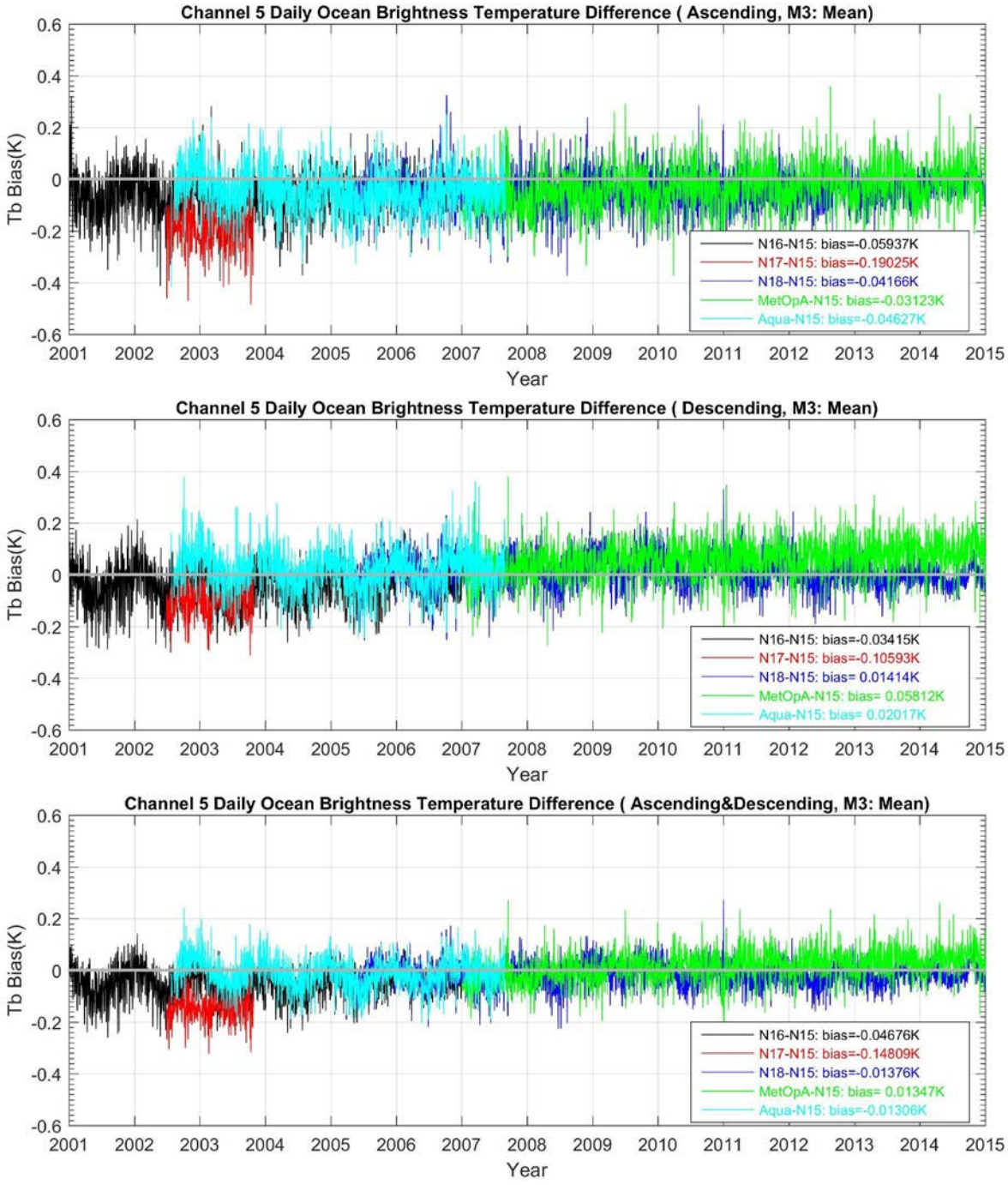

Figure 4-10 Time series of channel 5 daily ocean brightness temperature difference between satellite pairs of the mean gridded FCDR.

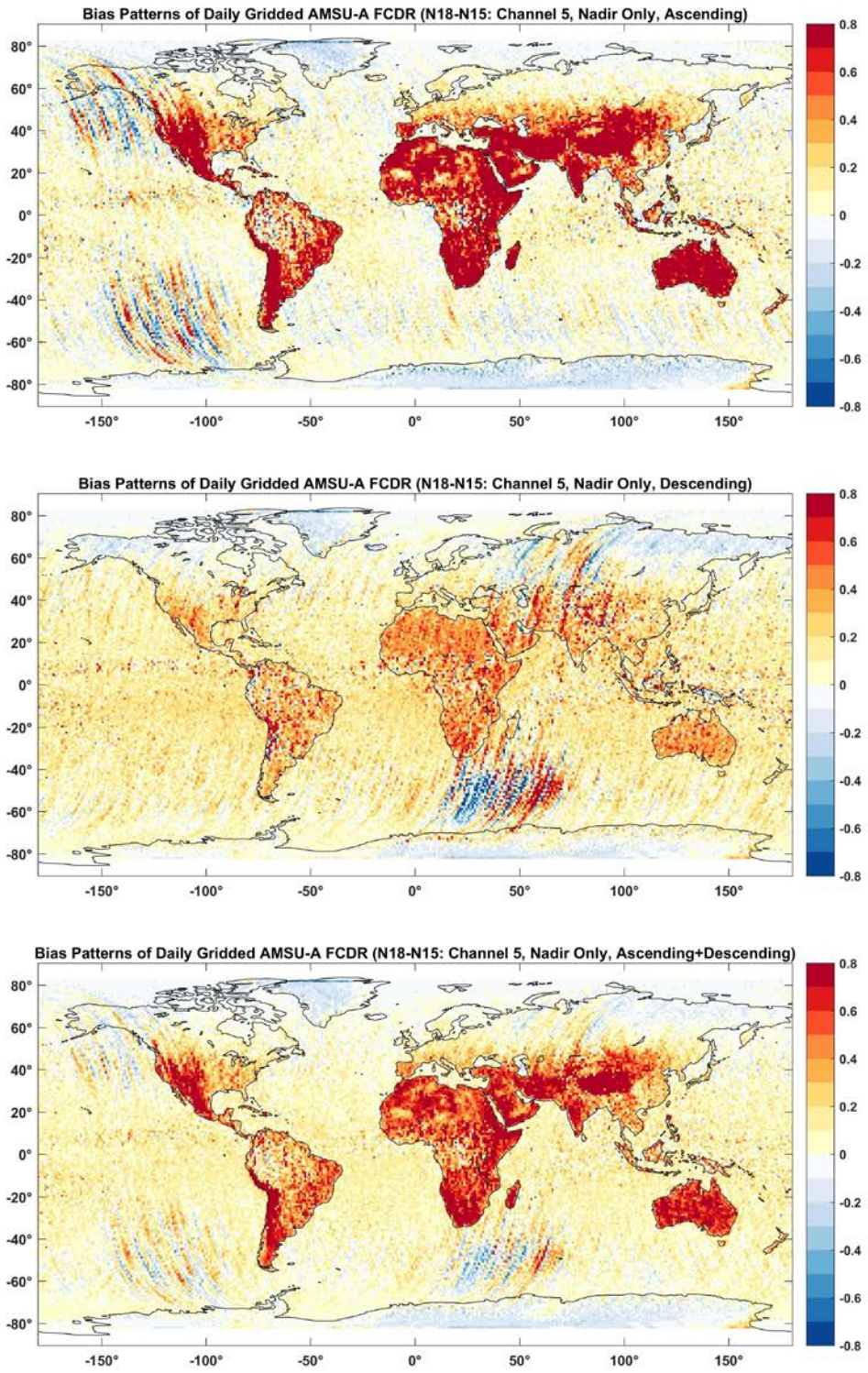

Figure 4-11 Spatial pattern of the channel 5 inter-satellite difference between N15 and N18 for the near-nadir only FCDR during January 2006-December 2014.

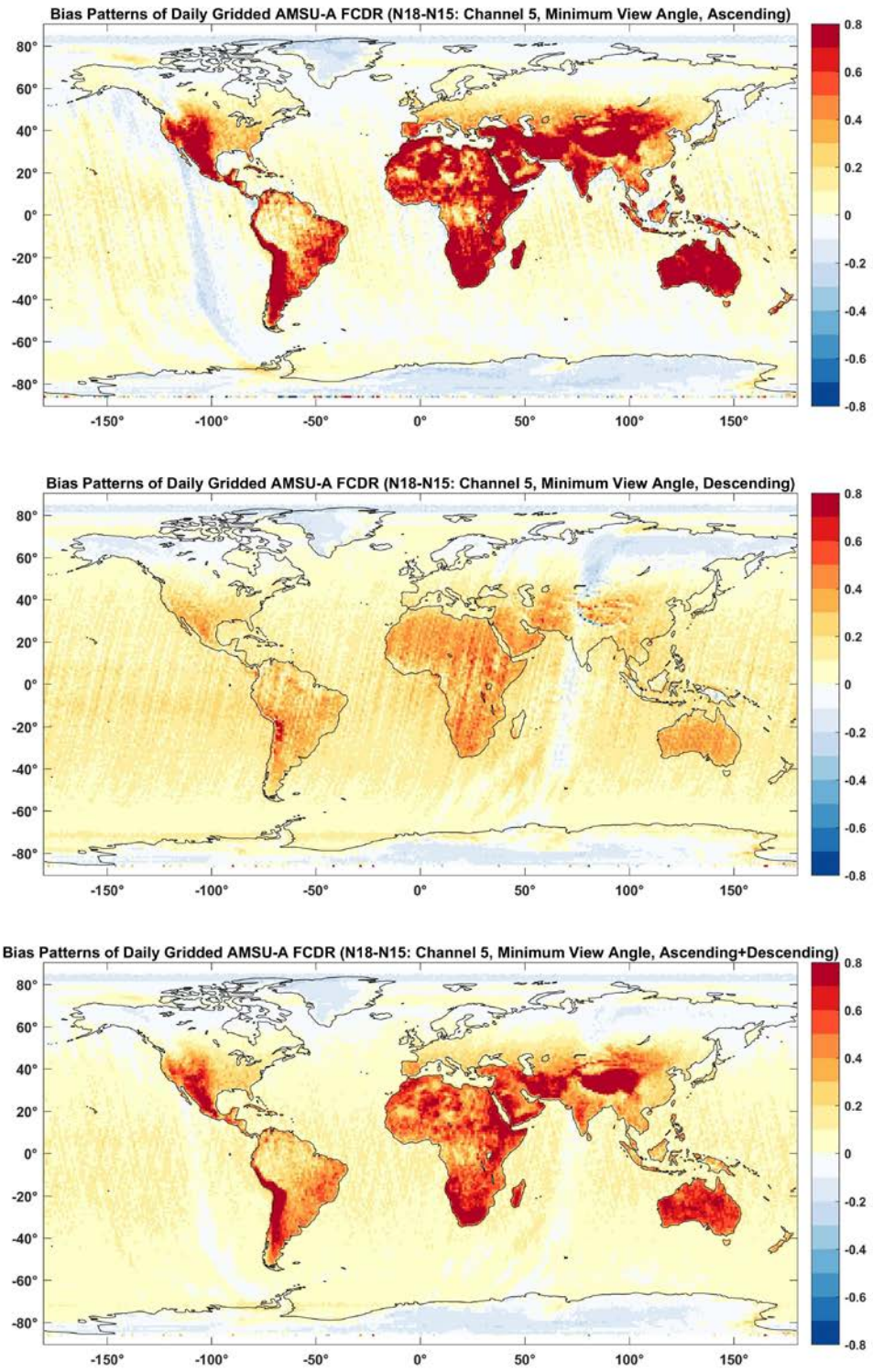

Figure 4-12 Spatial pattern of the channel 5 inter-satellite difference between N15 and N18 for the minimum-VZA gridded FCDR during January 2006-December 2014.

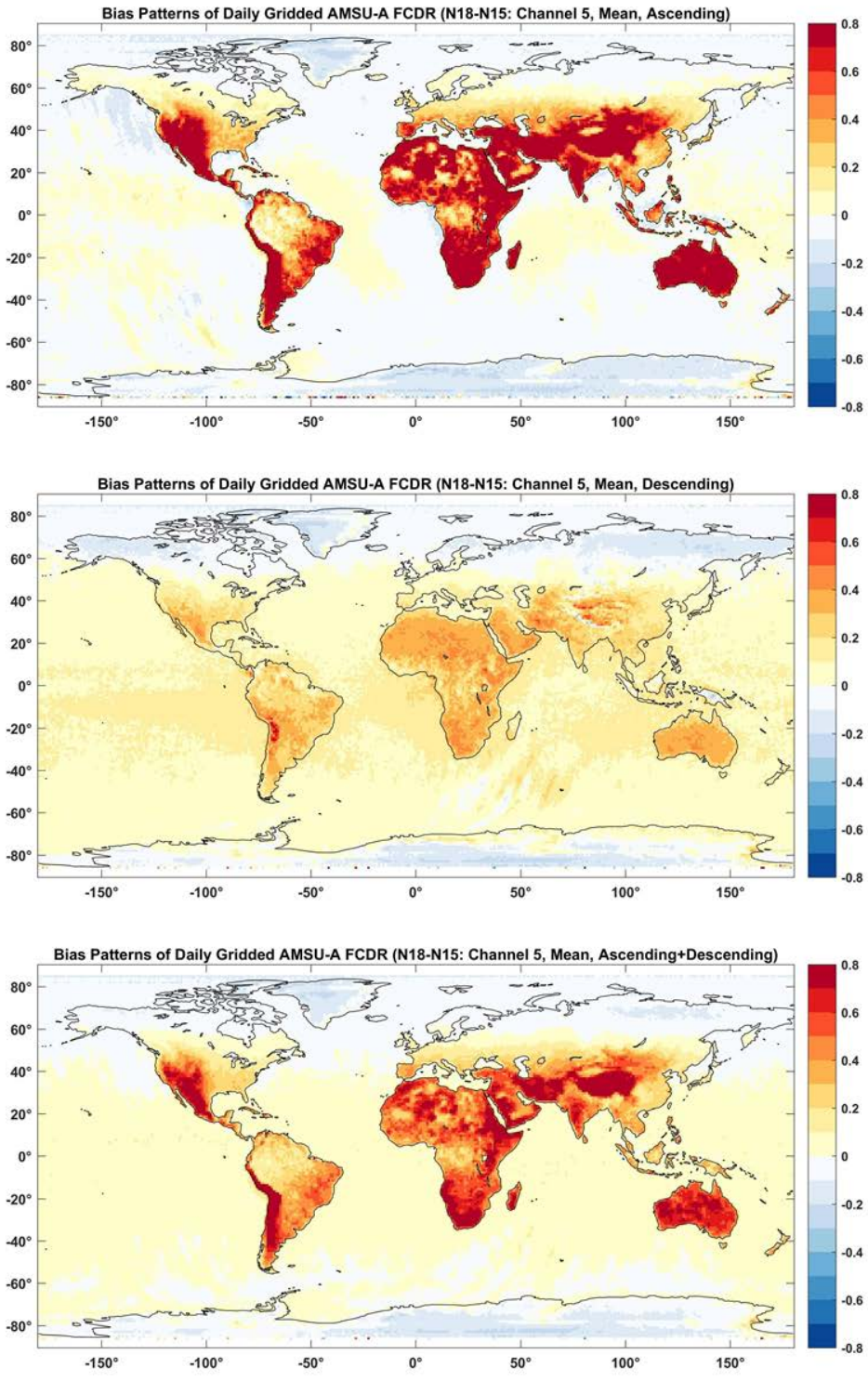

Figure 4-13 Spatial pattern of the channel 5 inter-satellite differences between N15 and N18 for the mean gridded FCDR during January 2006-December 2014.

4.2.3 Error Budget

Table 4-2 summarizes the errors in the SNO calibrated radiance FCDR. The accuracy of the gridded FCDR is the same as those of the original swath level-1c radiance FCDR.

Table 4-2 Error Budget in the IMICA calibrated radiances.

Error Type	Error Range	Comments
Calibration Uncertainty	0.5 - 1 K	This is total absolute uncertainty in instrument calibration.
Stability of Calibration Uncertainty	0.05-0.1 K/Decade	This stability is a measurement of bias drift relative to a benchmark climate observations that is considered as no error drift
Relative stability of Calibration Uncertainty	0.02 K/Decade	Relative bias drift between satellite pairs are small after bias drifts are minimized in the IMICA inter-calibration
Scene temperature dependent biases due to inaccurate calibration non-linearity	0.02 K/K	This is the worst case estimate for instrument channels that are not well represented by quadratic calibration equation. For most well calibrated satellite channels, this value can be as small as zero.
Noise equivalent temperature	0.2-0.3 K	This is a post-launch performance value for most channels. For AMSU channel 14, this value is about 0.6 K.
Global mean inter-satellite biases	0.1-0.2 K	
Standard deviation of global mean inter-satellite differences	0.03 K	This is the value for most tropospheric channels. For stratospheric channels, this value can reach 0.07-0.08 K for certain satellite pairs

4.2.4 Measurement Uncertainty Estimates

Measurement uncertainty is an estimate of absolute bias for any scan positions, which equals to absolute calibration bias plus noise equivalent temperature. Inter-calibrated radiances have similar calibration biases for different satellites, due to good performance of the IMICA approach as descried earlier. This allows reasonable estimates of measurement uncertainty for IMICA inter-calibrated radiances. This bias is estimated to be 0.5 K based on comparisons with GPSRO observations on AMSU-A channel 9 as seen in Section 4.2.2.2. More channel comparisons are being conducted as part of the IMICA inter-

calibration effort. If biases larger than 0.5 K are found between IMICA calibrated AMSU-A data and GPSRO observations, AMSU-A calibration offsets will be adjusted to bring the biases to be within 0.5K. As a result, a 0.5 K calibration bias is assumed for all IMICA calibrated MSU and AMSU-A channels.

MSU noise equivalent temperature is 0.3 K for all channels. With given calibration biases, the measurement uncertainty estimates for MSU are 0.8 K. AMSU-A noise equivalent temperatures for tropospheric channels are around 0.25-0.4 K (Mo 1996), but they can be as large as 0.8 to 1.2K for upper stratospheric channels (channels 13 and 14). This gives AMSU-A measurement uncertainty estimates about 0.75 to 0.9K for most tropospheric channels and 1.3-1.7 K for the upper stratospheric channels. These estimates are for IMICA inter-calibrated brightness temperatures only. Since calibration biases for operational calibrated brightness temperatures are different for different satellites, such uncertainty estimates are not provided for operational calibrated radiances.

5. Practical Considerations

5.1 Numerical Computation Considerations

Swath scene temperature fields dominate the storage requirements in the MSU/AMSU FCDRs. Compared to MSU (4 channels and 11 spots per scan line), AMSU-A has 15 channels and 30 footprints per scan line. Moreover, AMSU-A features a finer spatial resolution (45 km at nadir) than MSU (110 km at nadir). Under the same software and data design, the required disk space of AMSU-A is more than 20 times larger than that of MSU; the processing time for AMSU-A would also be more than 20 times longer. Therefore, different strategies were used to address disk space and processing time issues in MSU and AMSU-A.

1) **Data type of temperature fields**: MSU data volume is relatively small (~ 70 GB), hence all temperature fields are stored in floating point format (4 bytes), which is convenient for data users. For AMSU-A, brightness temperature field supports two formats: scaled integer (2 bytes) and floating point. Scaled integer format can reduce storage space to half of that required by floating point format. However data users need to convert the scaled integers to floating point numbers and the precision of temperatures is thus reduced (0.01 K, but still sufficient for climate trend studies). For AMSU-A daily gridded FCDR, since the spatial resolution of the data is 1°×1°, the file size is not big even with the single-precision floating-point format. As a result, brightness temperatures in the AMSU-A daily gridded FCDR are stored using the single-precision floating-point format.

2) **Parallelization**: To speed up the AMSU-A processing, multithreading technique was employed in its FCDR software code. This technique allows a computer program to run faster on a computer system that has multiple CPUs, CPU with multiple cores, or across a cluster of machines. The parallelization was implemented at level-1b file level, i.e., multiple AMSU-A level-1b files can be processed simultaneously to generate level-1c files. The software for producing the AMSU-A daily gridded FCDR was also parallelized using multi-thread technique to speed-up the processing.

5.2 Programming and Procedural Considerations

The MSU and AMSU-A FCDR software packages do not implement any numerical model.

5.3 Quality Assessment and Diagnostics

Percentage of missing/bad pixels in each level 1c file is monitored as an indicator of product quality. Missing or bad pixels are identified using the following diagnostics procedures:

(1) **Invalid level 1b file** is identified using NOAA Polar Orbiter Data User's Guide (for MSU) and KLM User's Guide (for AMSU-A) format specifications. If a header record error is identified, all scan lines will be flagged as bad.

(2) **Invalid time in level 1b files**. Two types of invalid time may exist in MSU and AMSU-A level 1b files: (1) invalid starting/ending time in header record; (2) invalid time in data record. A level 1b file with invalid starting and/or ending times will be flagged as bad file. A scan line with an invalid time will be flagged as bad scan line.

(3) **Invalid or missing geolocation**. Any pixel with an invalid or missing geolocation will be flagged as an invalid pixel.

(4) **Invalid or missing raw counts or warm target temperatures**. No calibration will be conducted in this case. Corresponding scene temperatures will be set to missing value (-9999) and its pixel level quality control flag will be set to 1.

(5) **Invalid scene temperatures**. All temperature values in MSU channels 2-4 and AMSU-A channels 4-14 will be compared to the Product Measurement Range given in Tables 2-1 and 2-2. Any pixel at any channel with invalid temperature will be replaced by missing value. Corresponding pixel level quality control flag will also be set to 1.

(6) **Precipitation screening**. Precipitation screenings for MSU channel 2 and AMSU-A channel 5 are implemented to screen out suspicious brightness temperatures associated with precipitation. Precipitation pixels will be replaced by missing values, and corresponding pixel level quality control flag will be set to 1.

For daily gridded products, not all the grid cells are covered by valid AMSU-A data. Spatial gaps exist, which are especially large for the near-nadir-only FCDR product. For grid cells without valid observations, invalid values are filled.

Overall product quality is also assessed by analyzing randomly selected daily mean images of the brightness temperatures of individual satellite. Suspicious temperatures over certain locations may suggest bad data have passed through the processing codes.

5.4 Exception Handling

Exceptions that were considered in the MSU and AMSU-A FCDR processing codes include:

(1) **Class Not Found Exception** will be reported and the system stops running when the AMSU-A processing code tries to load in a class but no definition for the class could be found due to misplacement of external libraries.

(2) **Out of Memory Exception** will be identified when the system cannot allocate a block a memory because it is out of memory. If this exception occurs, the system will report the exception and exit running.

(3) **File Not Found Exception** will be reported and the system exits running when a calibration coefficients file, a limb correction coefficient file, or the land type file does not exist. It will also be identified if the file does exist but for some reason is inaccessible.

(4) **EOF Exception** will be reported when an end of file has been reached unexpectedly during file reading operations. If this exception occurs during reading a level 1b file, the system will stop processing the file, report the exception, and continue to process the next file. If this exception occurs during reading a calibration coefficients file, a limb correction coefficient file, or the land type file, the system will exit running.

(5) **IO Exception** will be reported and the system stops running when a failed I/O operation, other than 3 and 4, occurs.

5.5 Processing Environment and Resources

Table 5-1 lists the environment and resource required by the MSU and AMSU-A FCDR processing codes. The processing environment and resources for generating the daily gridded AMSU-A FCDR products are listed in table 5-2.

Table 5-1 MSU and AMSU-A processing and environment and resource requirements.

	MSU	**AMSU-A**
Computer hardware	Minimum Configuration: Processor: 2.0 GHz Memory: 100 MB Disk space: 75 GB	Minimum Configuration: Processor: 2.0 GHz Memory: 200 MB Disk space: 900 GB A system with multiple CPUs is preferred.
Operating System	Linux	Linux, Windows NT/7, Solaris
Programming Language(s)	FORTRAN 77 bash script	Java bash script
Compilers	GNU Fortran 77 (g77)	Sun Java Compiler
External Libraries & Versions	NetCDF 3.6.1 (unidata)	NetCDF-java 4.1 (unidata) HDF Java from HDFView2.3 (for Aqua AMSU-A)
Storage Required (GB)	70	900 (scaled integer format)
Time Required (hour)	50 hours for 14 satellites	60 hours for 6 satellites in parallel computation

Table 5-2 Processing and environment and resource requirements for generating AMSU-A daily gridded FCDR products.

Item	Requirement
Computer hardware	Minimum configuration: Processor: 2.0GHZ Memory: 8G Disk space: 2T
Operating system	Linux Windows Unix
Programming language	Java, Shell Script
Complier	Java compiler
External library and version	NetCDF-Java 4.6 and above
Storage	2T
Time Required	Around 80 hours for 6 satellites with single threaded processing. For parallel processing, depends on number of threads used.

6. Assumptions and Limitations

6.1 Algorithm Performance

There are two fundamental assumptions associated with the calibration algorithm: a) the end-to-end calibration of the instrument can be described by a quadratic calibration equation; b) post-launch information required to obtain the calibration coefficients have been correctly used.

On the first assumption, there are possibilities that the calibration equation is not a quadratic type for certain channels and sensors. Higher order terms in the calibration equations may exist. In this situation, two calibration coefficients are not sufficient to characterize the nature of instrument biases. Scene temperature dependent biases may occur since they cannot be removed by the calibration algorithm of the quadratic type (Zou et al., 2009).

Including high order terms than quadratic in the calibration equation is difficult since there is lack of information to determine the calibration coefficients for the high order terms. Depending on the applications of the radiance datasets, empirical bias correction schemes shall be carried out for the biases unresolved in the IMICA calibration.

On the second assumption, the calibration coefficients are determined by minimizing inter-satellite biases including scene temperature dependency in biases, instrument temperature dependency in biases, and bias drifts. It is possible that other types of biases still exist that require introduction of more calibration coefficients or change of the current calibration coefficients. Once these unknown types of biases are discovered, further investigation of the validity of the calibration algorithm and coefficients are required.

The gridded FCDR products are generated using straightforward spatial gridding algorithms. These algorithms are simple and well defined. No changes are expected. In case an error incurs in the gridded FCDR products, it will most likely be caused by the quality of the input L1c FDCR data or sensor degradation, not by the gridding algorithms.

6.2 Sensor Performance

This C-ATBD discusses the radiance FCDR and daily gridded FCDR which fundamentally rely on sensor performance. The sensor performance including radiometric noise equivalent temperature, calibration, spatial and spectral errors which have been discussed in the validation and accuracy section (Section 4). A summary of the performance is listed in Table 4-2, which is based on the assumption that geophysical effects or the targets being observed do not affect the sensor performance. In the last few years, STAR has developed an Integrated Calibration Validation System (ICVS) for monitoring sensor performance for operational NOAA satellites. Currently, AMSU-A sensors onboard NOAA-15, NOAA-18, NOAA-19, MetOp-A and MetOp-B series are monitored by the ICVS on a daily basis. In case the FCDR products incur a quality problem, possible reasons related to sensor performance can be examined using the ICVS.

7. Future Enhancements

Possible future enhancement of the radiance FCDR algorithm may include absolute calibration, warm target and cold target calibrations, as described in the following.

7.1 Enhancement 1: Absolute calibration

Although inter-satellite differences have been minimized by the IMICA calibration, the absolute values of the MSU/AMSU multi-satellite level-1c radiances contain a constant bias relative to an unknown absolute truth. This bias is estimated to be 0.5 to 1 K. This constant bias does not affect the variability and trend analysis of the subsequent products developed from the FCDR. However, it affects data assimilations in climate reanalyses and NWP forecasting. This bias needs to be determined in FCDR validation processes against certain reference observations, ideally SI-traceable standards. Future enhancement in this area includes development of validation plans as part of the MSU/AMSU FCDR development effort. This includes comparisons against GPS RO observations as well as observations from the Global Climate Observing System Upper-Air Network. However, because all observations feature certain errors, there is no guarantee that such comparisons will result in the absolute temperature values with required accuracies. Ultimately, community consensus references for absolute calibration need to be developed, which still remains a challenging task.

7.2 Enhancement 2: target calibrations

In the current algorithm, the side-lobe effect of the cosmic space cold target has been assumed to be a constant about 2K for both MSU and AMSU-A channels. However, this effect is a function of time and channels. Future enhancement on this area includes development of more sophisticated cold target calibration algorithms for more accurate level-1c radiance derivation.

The warm target temperature is currently assumed to be the average of available good PRT measurements. However, inhomogeneous heating of the warm target causes warm target thermal gradient; as a result, different PRT measurements on different warm target locations give different temperatures at the same time. This warm target thermal gradient problem causes warm target anomalies on short term time scales. It is desirable to understand how this problem affects accuracies of level-1c radiance calibration. Future enhancement in this area will include development of a more sophisticated warm target calibration algorithm with thermal gradient effect incorporated and then an understanding of its impact on accuracies of level-1c radiances.

8. References

Cao, C., et al. (2004). Predicting Simultaneous Nadir Overpasses among Polar-Orbiting Meteorological Satellites for the Intersatellite Calibration of Radiometers. Journal of Atmospheric and Oceanic Technology, 21(4), 537-542

Kidwell, K.B., edited, (1998). NOAA Polar Orbiter Data User's Guide, available at http://www.ncdc.noaa.gov/oa/pod-guide/ncdc/docs/podug/index.htm

Mo, T. (1996). Prelaunch calibration of the advanced microwave sounding unit-A for NOAA-K. Microwave Theory and Techniques, IEEE Transactions on, 44(8), 1460-1469

Mo, T. (2006). Calibration of the Advanced Microwave Sounding Unit-A Radiometers for METOP-A, NOAA Technical Report NESDIS 121. Washington DC: NOAA/NESDIS/STAR

Robel, J., et al. edited, (2009). NOAA KLM user's guide, available at http://www.ncdc.noaa.gov/oa/pod-guide/ncdc/docs/klm/index.htm

Saha, S., et al. (2010). The NCEP climate forcast system reanalysis. Bulletin of the American Meteorological Society, 91(8), 1015-1057

Rienecker, M. M., et al. (2011), MERRA: NASA's Modern-Era Retrospective Analysis for Research and Applications, J. Clim., 24, 3624–3648, doi:10.1175/JCLI-D-11-00015.1.

Zou, C.-Z., et al. (2009). Error structure and atmospheric temperature trends in observations from the Microwave Sounding Unit. Journal of Climate, 22(7), 1661-1681

Zou, C.-Z., et al. (2006). Recalibration of microwave sounding unit for climate studies using simultaneous nadir overpasses. Journal of Geophysical Research, 111(D19), D19114

Zou, C.-Z., & Wang, W. (2010). Stability of the MSU-derived atmospheric temperature trend. Journal of Atmospheric and Oceanic Technology, 27(11), 1960-1971

Zou, C.-Z., & Wang, W. (2011). Intersatellite calibration of AMSU-A observations for weather and climate applications. J. Geophys. Res., 116(D23), D23113

Wang, W., and C.-Z. Zou (2014). AMSU-A-Only Atmospheric Temperature Data Records from the Lower Troposphere to the Top of the Stratosphere. J. Atmos. Oceanic Technol., 31, 808-825, DOI: 10.1175/JTECH-D-13-00134.1

Appendix A. Acronyms and Abbreviations

Acronym or Abbreviation	Meaning
AMSU	Advanced Microwave Sounding Unit
AMSU-A	Advanced Microwave Sounding Unit-A
ATBD	Algorithm Theoretical Basis Document
BT	Brightness Temperature
CATBD	Climate Algorithm Theoretical Basis Document
CDR	Climate Data Record
CDRP	Climate Data Record Program
CHAMP	CHAllenging Minisatellite Payload
CFSR	Climate Forecast System Reanalysis
COSMIC	Constellation Observing System for Meteorology Ionosphere & Climate
ECMWF	European Centre for Medium-Range Weather Forecast
EOS	Earth Observing System
EUMETSAT	European Meteorological Satellite Agency
FCDR	Fundamental Climate Data Record
FOV	Field of View
GPS	Global Positioning System
GRACE	Gravity Recovery And Climate Experiment
IFOV	Instantaneous Field of View
IMICA	Integrated Microwave Inter-Calibration Approach
IR	Infrared
JPSS	Joint Polar Satellite System
LEO	Low Earth Orbit
LZA	Local Zenith Angle
MERRA	Modern Era Retrospective-analysis for Research and Applications
MetOp-A	European Meteorological Operational satellite programme
MSU	Microwave Sounding Unit
NASA	National Aeronautics and Space Administration
NCDC	National Climatic Data Center
NESDIS	National Environmental Satellite, Data, and Information Service
NCEP	National Centers for Environmental Prediction

NeDT	Noise Equivalent Difference of Temperature
NIR	Near Infrared
NOAA	National Oceanic and Atmospheres Administration
NPOESS	National Polar-orbiting Operational Environmental Satellite System
NWP	Numerical Weather Prediction
PRT	Platinum Resistance Thermometer
RAOB	Radiosonde Observation
RMSE	Root Mean Square Error
RO	Radio Occultation
SAC-C	Satellite de Aplicaciones Cientificas-C
SNO	Simultaneous Nadir Overpass
STAR	Center for Satellite Applications and Research
TCDR	Thematic Climate Data Record
TOVS	TIROS Operational Vertical Sounder